KANATLARIN DAİMİ VE DAİMİ OLMAYAN AERODİNAMİĞİ

YÜKSEK LİSANS TEZİ

Müh. Kerim Can BAYAR

Anabilim Dalı : UZAY BİLİMLERİ VE TEKNOLOJİSİ
Program : UZAY

TEMMUZ 1991

STEADY AND UNSTEADY

AERODYNAMICS OF WINGS

M. Sc. THESIS

KERIM CAN BAYAR, B. Sc.

Date of Submission : June 10, 1991
Date of Approval : July 9, 1991

Examination Committee

Supervisor : Assoc.Prof.Dr. C. Ruhi KAYKAYOGLU
Member : Prof.Dr. Umur DAYBELGE
Member : Assoc.Prof.Dr. Adil YUKSELEN

JULY, 1991

ABSTRACT

Modern fighter aircraft operation at high angle of attack, during take-off, landing and unsteady maneuvering, is dominated by the interaction of vortical type flows and lifting surfaces. In such flight conditions, unsteadyness and flow separation can produce nonlinear aerodynamic effects which significantly influence the instantaneous load distribution on the lifting surfaces and controllability of the aircraft. Numerically simulation of unsteady aerodynamics and the wake dynamics is therefore much needed in flight dynamics and for structural load analysis.

The application range of the present code consists of the steady wing theory and also unsteady wing theory solutions. It includes non-iterative technique for wake development and prediction of the time dependent aerodynamic characteristics in both incompressible and compressible flow. Also results consist of comparison between steady and unsteady solutions with arbitrary wing planforms. The output of the present code is the aerodynamic flow characteristics around the geometry such as the velocity and pressure distributions, mach contours, forces and moments.

JULY 1991   Kerim Can BAYAR

CONTENTS

NOMENCLATURE

a_p	Panel chord length
a_w	Influence coefficient of wing doublet distribution
a_{we}	Influence coefficient of edge vortices along the edges of the wing panel
a_{wp}	Influence coefficient of vorticity distribution on the wing panel
A_i	Chord length of the wing at the collocation point
$[A_b]$	Matrix of velocity influence coefficients representing influence of wing doublet distribution relative to the wing panel
$[A_l]$	Matrix of velocity influence coefficients representing influence of leading-edge doublet distribution relative to the wing panel
$[A_t]$	Matrix of velocity influence coefficients representing influence of trailing-edge doublet distribution relative to the wing panel
$[A_{bw}]$	Matrix of velocity influence coefficients representing influence of wing doublet distribution relative to the wake panel
$[A_{lw}]$	Matrix of velocity influence coefficients representing influence of other leading-edge doublet distribution relative to the wake panel
$[A_{tw}]$	Matrix of velocity influence coefficients representing influence of other trailing-edge doublet distribution relative to the wake panel
b_w	Influence coefficient of wing source distribution
c	Wing chord length
C_D	Drag coefficient
C_L	Lift coefficient
C_ℓ	Rolling moment coefficient
C_m	Pitching moment coefficient
C_p	Pressure coefficient
e_x, e_y, e_z	Unit vector components
$\vec{F}$	(F_x, F_y, F_z) Force divided by free stream dynamic pressure on the configuration in (x,y,z) coordinate system
F_1, G_1, G_2, G_3	Elementary functions in incompressible flow
$F_{1c}, G_{1c}, G_{2c}, G_{3c}$	Elementary functions in compressible flow
h	Panel vertical distance from x axis
K	Switch factor in compressible flow

M_∞	Free stream Mach number
P	Static pressure
P_∞	Static pressure in free stream
p,q,r	Angular velocity about x,y,z axes, respectively
q_l, q_t	Source distribution on the panel's leading-edge and trailing-edge, respectively
$\vec{r}$	Distance vector
S	Wing area
S_{x^*}, S_{z^*}	Path components in a inertial co-ordinate system
t	Time
$U(t)$	Time dependent wing forward velocity
u,v,w	Induced velocity in the x,y and z directions, respectively
U_{sc}	Velocity induced by constant source distribution on a wing panel
U_{sl}	Velocity induced by leading-edge source distribution
U_{st}	Velocity induced by trailing-edge source distribution
U_{dle}	Velocity induced by edge vortices of leading-edge doublet distribution on a wing and/or wake panel
U_{dte}	Velocity induced by edge vortices of trailing-edge doublet distribution on a wing and/or wake panel
U_{dlp}	Velocity induced by leading-edge doublet distribution on a wing and/or wake panel
U_{dtp}	Velocity induced by trailing-edge doublet distribution on a wing and/or wake panel
x,y,z	Wing coordinates in a non-inertial co-ordinate system
x^*,y^*,z^*	Wing coordinates in a inertial co-ordinate system
x_{le}, x_{te}	Equation of panel leading-edge and trailing-edge
α	Angle of attack
β	Tangent of sweep of Mach lines
Γ	Strength of the doublet circulation
θ	Inclination angle of wing panel
v_k	Tangent of the sweep angle of leading and trailing edge of wing panel
ρ	Density
ϕ	Velocity potential
ω	Time dependent angular velocity vector

∇	Denotes the gradient with respect to x
[ ]	Denotes a matrix
$\rightarrow$	Denotes a vector with three components in x,y,z
k	Denotes contributions from four corner points of panel as a subscript or superscript
i	Denotes the contributions from each panel
l	Denotes the number of unknown leading-edge doublet parameters
m	Denotes the number of unknown trailing-edge doublet parameters
n	Denotes the number of unknown wing doublet parameters
0	Denotes the quantity at $t = 0$

LIST OF FIGURES

SUMMARY

The present method is a method for converting steady-state, potential flow based panel methods into a time dependent mode. Also this method permits both leading-edge and trailing-edge separation. Furthermore, the present method can provide transient aerodynamic loads and wake geometries during the time-dependent motion and improves the understanding of some vortex interaction problems. The free stream flow must be at small angle of attack and sideslip. The free stream Mach number must be sufficiently far from unity.

The flow around the configuration at a time step is simulated by a source distribution on the wing reference plane and doublet distribution on the wing and wake components. By the zero normal velocity condition at collocation points, a system of linear equations is obtained and solved by a direct method. As above calculations are completed the wake deformation is simulated by calculating the downwash at each wake element edge location. And then wake element moves with this downwash to new location. To conclude the calculation procedure for a given time step, the forces and moments are indicated by nonsteady Bernoulli equation. The above calculational scheme is then repeated for the additional time intervals. This scheme is numerically stable since iterative calculations are not required.

ÖZET

KANATLARIN DAİMİ VE DAİMİ OLMAYAN AERODİNAMİĞİ

Birçok mühendislik probleminin çözümünde kullanılmaya başlanan bilgisayarlar, tasarımcılara büyük kolaylıklar sağlamaktadır. Bilgisayar teknolojisinin gelişimine paralel olarak ilerleyen sayısal çözüm yöntemleri de deneysel imkanları daha kısıtlı ve külfetli olan alanlarda özellikle hava taşıtlarının aerodinamik tasarımlarında büyük aşamalar kaydettirmektedir.

Son birkaç yılda, akışkanlar mekaniğinde girdaplı akışların sıhhi analizleri ve gerçekçi tahminleri, helikopter, roket ve savaş uçaklarının modern dizaynları ile uğraşmakta olan aerodinamikçiler için çok önemli olmaya başlamıştır. Modern savaş uçakları iniş, kalkış, savunma ve hücum manevralarında, yüksek hücum açılarında zamana bağlı yörüngeler çizmektedir. Bu hücum açılarında, girdap yapılı akışlar, uçak etrafında aerodinamik karakteristikleri ve kontrol kabiliyetini ciddi bir şekilde etkileyebilmektedir.

Kompleks uçak manevralarının analizleri için geliştirilmekte olan hesaplamalı metodlarda, özellikle daimi olmayan aerodinamiğin simülasyonu ve ard iz bölgesi dinamiğinin oluşturulması hala popüleritesini korumaktadır. Bu zamana bağlı akışkanlar dinamiği modellemesi; zamana bağlı yapısal yük analizi, uçuş simülasyonu ve uçuş dinamiği gibi havacılık disiplinleri için çok gereklidir. Daimi olmayan aerodinamik üzerindeki çalışmalar gerek yoğun hesaplama ihtiyaçları gerekse zamana bağlılıktan gelen yan faktörleri ile daimi akışların yanında hala gizemini ve önemini koruyan bir alan olarak durmaktadır. Daimi olmayan aerodinamik için sıkıştırılamaz ve sübsonik (ses-altı) rejimlerde uygulanan değişik metodlar, transonik ve süpersonik (ses-üstü) rejimlere geçildiğinde azalmakta ve hassasiyetini korumaktadır.

Akışın fiziksel alanını tanımlamak ve bu bölge üzerinde karakteristik değerler elde etmek için kullanılan akışkanlar mekaniği denklemleri en kompleksinden en basitine doğru şu şekilde sıralanabilir:

- Navier-Stokes denklemleri
- Euler denklemleri
- Potansiyel denklemler

Navier-Stokes denklemleri, herhangi bir hücum açısı ve hızda herhangi bir konfigürasyonun üzerinde tanımlanabilen her türlü akış özelliklerini içerebilmektedir. Şok dalgalarının konumu, girdap tabakalarının ve geniş ölçekli ayrılmaların görüntülenmesi mümkündür. Karmaşıklığı nedeniyle

kompleks konfigürasyonlar üzerinde hala tam olarak çözüm içeren bir kod geliştirilmemiştir. Bu nedenle Navier-Stokes denklemlerini kapsayan kodlar daha çok bölgesel yaklaşımlar kullanmaktadır. **Euler denklemleri**, taşınım terimleri ve viskoz terimlerin ihmal edilmesi ile oluşturulur. Şok dalgasının konumu için bir ilk yaklaşım verebilmekte fakat viskoz terimlerin ihmal edilmesi nedeniyle ayrılma bölgelerinin görüntülenmesinde zorlanmaktadır. Eğer akış, daimi ve irrotasyonel kabul edilirse hız potansiyeli kavramı ortaya çıkar ve Euler denklemleri tekil **Potansiyel denklemine** dönüştürülebilir. Potansiyel denklem, güçlü şok dalgalarının ve akım ayrılmasının geniş ölçekli gerçekleşmediği akış alanlarında rahatlıkla kullanılabilen ve konfigürasyon karakteristikleri için ilk yaklaşım değerleri verebilen bir denklemdir. Bu denkleminin lineerleştirilmiş hali üzerine inşa edilen "Panel Metodları" ciddi bir rağbet görmektedir.

Bu tezde, aerodinamiğin iki kolu olan daimi ve daimi olmayan yapılar, Potansiyel denklem temel alınarak incelenmiş ve daimi aerodinamik için oluşturulan bir panel kodu ile zamana bağımlılığa geçilmeye çalışılmıştır.

Daimi aerodinamik için kullanılan panel metodu, lineerleştirilmiş potansiyel denkleminin (Prandtl-Glauert) çözülmesi esasına dayanır. Yerel hızın serbest akım hızından çok az saptığı akışlar için potansiyel denklemi, bir bozuntu hızı tanımlanarak daha basit ikinci dereceden bir lineer denkleme, Prandtl-Galuert denklemine dönüşür. Prandtl-Galuert denkleminin çözümünde kullanılan ana metot, yüzey tekillikleri teknikleridir. Cisim etrafındaki potansiyel akım Green teoremine göre kaynak ve duble gibi yüzey tekillikleri ile tanımlanabilir. Bu yüzey tekilliklerinin birbiri üzerine indüklediği hızları belirleyen aerodinamik etki katsayılarının hesaplanması metodun esasını oluşturmaktadır. Aerodinamik etki katsayılarını belirleyen integraller yüzey tekilliklerine yapılan yaklaşımlar ile çözülmektedir. Her panel için panel yüzeyinde normal yöndeki hızın sıfır olma koşulu sağlanarak, matris katsayılarını aerodinamik etki katsayılarının oluşturduğu bir denklem sistemi ortaya çıkmaktadır. Bu denklem sistemi çözüldükten sonra yüzey tekilliklerinin şiddetleri bulunmaktadır. Ayrıca her kanat panelinin firar kenarında Kutta şartı sağlanmakta ve kanat elemanının arkasında sonsuza uzanan düzlemsel bir ard iz paneli tanımlanmaktadır. Bu ard iz paneli üzerinde sabit büyüklükte bir duble tekilliği olduğu kabul edilmektedir.

Daimi olmayan aerodinamik için kullanılan metod aynı Panel Metodu üzerine inşa edilmiştir. Dolayısıyla sınır şartları pek değişmemekle birlikte denklemlere zamana bağımlılık terimleri eklenmektedir. Cisim üzerinde aerodinamik etki katsayıları matrisi oluşturulduktan sonra aynı şekilde yüzey tekilliklerinin şiddetleri bulunmakta daha sonra da bu tekillik şiddetlerine bağlı olarak firar ve/veya hücum kenarından kenar üzerindeki panel tekillik şiddetine eşit şiddette ard iz paneli oluşturularak atılmaktadır. Bu ardiz paneli üzerindeki hız da etki katsayılarından oluşan ikinci bir denklem sistemi ile çözülmektedir. En önemli fark daimi akım metodunda kullanılan sabit ardiz bölgesi geometrisinin değişken tabiatta olmasıdır.

Her iki halde de bir kanat paneli üzerindeki duble tekilliği, panel üzerindeki bir girdaplılık dağılımı ile panel iç ve dış kenar girdaplarının toplamından ibarettir. Her panel tüm tekilliklerden indüklenen değerlerin etkidiği bir kontrol noktası bulunmaktadır ve bu kontrol noktası panellerin orta noktası olarak alınmaktadır.

Her iki hal için de metodun içeriği ve önemli noktaları hakkında bilgi verdikten sonra genel denklem ve sınır şartlarını vererek, aerodinamik etki katsayılarının belirlenmesi sonucunda ilerlenecek adımları birer birer göstermeye çalışalım.

Lineerleştirilmiş potansiyel denklem, bilindiği gibi

$$\nabla^2 \phi = 0$$

şeklinde ifade edilebilmektedir. Yüzey üzerinde hızın sıfır olması ve bozuntunun kanat yüzeyinden çok uzakta olduğu şartı göz önüne alınacak olursa transforme edilmiş sınır şartları,

$$\left.\frac{\partial \phi_c}{\partial z}\right|_{z=0} = \left[U(t)+\frac{\partial \phi}{\partial x}\right]\frac{\partial h}{\partial x} + \frac{\partial h}{\partial t} - \frac{\partial \phi_w}{\partial z} + \omega.x \equiv W_{i,j}$$

$$\nabla \phi_o \rightarrow 0 \quad as \quad |x|,|y|,|z| \rightarrow \infty$$

yukarıdaki gibi ifade edilebilmektedir. Burada potansiyel fonksiyonunun z doğrultusunda türevini alırsak,

$$W_{i,j} = -\left[(U(t)-r.y).\left(\frac{\partial h}{\partial x}-\sin\alpha_i\right)-q.x + p.y + \frac{\partial h}{\partial t}\right]$$

şeklinde elde ederiz. Bu denklem üzerinde (p,q,r), (x,y,z) eksenleri etrafında kanat geometrisinin açısal hareketi, U(t) kanat geometrisinin zamana bağlı serbest akım hızı, h(t) ise panellerin zaman içerisinde x ekseni ile yaptığı dik uzaklık olarak tanımlanmaktadır. Görüldüğü gibi kanat geometrisinin zamana bağımlı hareketini bu denklem sistemi ile verebilmek oldukça kolaylaşmaktadır. Aynı şekilde kanat panelleri ile firar ve hücum kenarından ayrılan panellere ait yüzey tekilliklerinin z doğrultusunda türevleri alınırsa oluşacak olan matris sistemi,

$$\left(\frac{\partial \phi}{\partial z}\right)_{ij} = [A_b]\begin{vmatrix} i=1 \\ \vdots \\ \Gamma_{b_i} \\ \vdots \\ i=n \end{vmatrix} + [A_l]\begin{vmatrix} i=1 \\ \vdots \\ \Gamma_{l_i} \\ \vdots \\ i=l \end{vmatrix} + [A_t]\begin{vmatrix} i=1 \\ \vdots \\ \Gamma_{t_i} \\ \vdots \\ i=m \end{vmatrix}$$

yukarıdaki gibidir. Bu denklem sisteminde,

[A$_b$] matrisi; kanat yüzey tekilliklerinin kanat panellerine etkisi

[A$_l$] matrisi; hücum kenarı ayrılmış panel yüzey tekilliklerinin kanat
    panellerine etkisi

[A$_t$] matrisi; firar kenarı ayrılmış panel yüzey tekilliklerinin kanat
    panellerine etkisi

olarak tanımlanabilir. Toplam z doğrultusunda hızın sıfır olması şartı, denklem sistemini aşağıdaki şekle dönüştürür.

$$(U-r.y)\left(\frac{\partial h}{\partial x}-\sin\alpha_i\right)-q.x+p.y+\frac{\partial h}{\partial t}$$

$$= [A_b]\cdot\begin{vmatrix}\Gamma_{b_i}\end{vmatrix} + [A_l]\cdot\begin{vmatrix}\Gamma_{l_i}\end{vmatrix} + [A_t]\cdot\begin{vmatrix}\Gamma_{t_i}\end{vmatrix}$$

Yukarıdaki denklem sisteminde sol taraf kanat geometrisinin hareketi tanımlandığı taktirde bilinmektedir. t=0 anı için firar ve hücum kenarı matrisleri de doğrudan sıfır olacağına göre, [A$_b$] matrisi kolaylıkla çözülebilmektedir. Elde edilen kanat yüzey tekilliklerinden, firar ve hücum kenarı üzerinde bulunan paneller üzerindeki yüzey tekillik şiddetleri firar ve hücum kenarından ayrılmak üzere olan panel şiddetlerine eşittir. Dolayısıyla atılacak olan her bir panel üzerindeki yüzey tekillik şiddeti bir önceki adım şiddetinden bilinmektedir. Buna bağlı olarak firar ve hücum kenarları panelleri 1/2UDt oranında ötelenirler. Paneller üzerindeki köşe noktalarının hız bileşenleri ise,

$$(u,v,w)_i = [A_{bw}]\cdot\begin{vmatrix}\Gamma_{b_i}\end{vmatrix} + [A_{lw}]\cdot\begin{vmatrix}\Gamma_{l_i}\end{vmatrix} + [A_{tw}]\cdot\begin{vmatrix}\Gamma_{t_i}\end{vmatrix}$$

denklem sisteminin çözümü ile bulunmaktadır. Bu denklem sisteminde,

[A$_{bw}$] matrisi; kanat panellerinin ardiz panellerine etkisi

[A$_{lw}$] matrisi; Diğer hücum kenarı panellerinin ardiz panellerine etkisi

[A$_{tw}$] matrisi; Diğer firar kenarı panellerinin ardiz panellerine etkisi

olarak belirlenmektedir. Her iki denklem sisteminde dikkat edilmesi gereken nokta, kanat panelleri etki katsayıları matrisinin bütün zaman adımları içerisinde N boyutunda kalırken, firar ve hücum kenarından atılmakta olan panellerin aerodinamik etki katsayılarını içeren matrisler sırasıyla M ve L boyutunda başlıyarak her bir hesaplama adımında M ve L adet artmaktadır. Dolayısıyla [A$_b$] matrisi eğer kanat geometrisinin şekli zaman içerisinde değişmiyorsa bir defaya mahsus hesaplanmakta ondan sonra her zaman adımında daima aynı matris kullanılmaktadır. Yukardaki son denklem ile M+L adet panelin köşe noktalarında hız değerleri hesaplandıktın sonra paneller yeni konumlarına,

$$\left(\Delta x, \Delta y, \Delta z\right)_i = \left(u, v, w\right)_i \cdot \Delta t$$

ilerletme denklemi ile ulaştırılırlar. Bu yeni konum altında daimi olmayan terimlerinde içerildiği Bernoulli denklemi çözülerek basınç alanı,

$$\frac{P_\infty - P}{\rho} = (U - r \cdot y)\frac{\partial \phi}{\partial x} + \frac{\partial \phi}{\partial t} + \frac{1}{2}\left[\left(\frac{\partial \phi}{\partial x}\right)^2 + \left(\frac{\partial \phi}{\partial y}\right)^2 + \left(\frac{\partial \phi}{\partial z}\right)^2\right]$$

buna bağlı olarak kuvvet alanı,

$$\Delta F_i = 2\rho\left(U\int_{x_i}^{x_{i+1}} \frac{\partial \phi}{\partial x} \cdot dx + \int_{x_i}^{x_{i+1}} \frac{\partial}{\partial t}\int_0^x \frac{\partial \phi}{\partial x} \, dx \cdot dx\right)$$

ve tek tek kuvvet ve moment değerleri bulunmaktadır.

$$C_L = \sum_{i=1}^{n} \Delta F_i \cdot \cos \alpha_i \Big/ \frac{1}{2}\rho U^2 S$$

$$C_D = \sum_{i=1}^{n} \Delta F_i \cdot \sin \alpha_i \Big/ \frac{1}{2}\rho U^2 S$$

$$C_m = \sum_{i=1}^{n} \cdot \Delta F_i \, x_i \Big/ \frac{1}{2}\rho U^2 S.c$$

$$C_\ell = \sum_{i=1}^{n} \Delta F_i \cdot y_i \Big/ \frac{1}{2}\rho \cdot U^2 S.c$$

Yukarıdaki hesaplamalar bir defa yapıldıktan sonra firar ve hücum kenarlarından atılan panellerin yeni konumları ile baştaki denkleme tekrar dönülerek aynı yol tekrar izlenir. Bu tür bir yöntem iteratif bir teknik olmadığı için hem daha hızlı ve matris büyüklüğü daha az hem de daha kararlıdır.

Yukarıda kısaca özetlenmeye çalışılan metot, daimi olmayan aerodinamik problemlerine daimi bir yaklaşım getirdiği için önem taşımaktadır. Bu tez çerçevesinde, herhangi bir kanat geometrisi etrafında üç boyutlu akım daimi akış olarak incelenmiş ve tüm akış karakteristikleri çıkarılmıştır. Daha sonra aynı geometri ile daimi olmayan bir akış altında karakteristikler üzerindeki değişimler incelenmiştir. Tezin sonuç bölümünde çıktılar detaylı bir şekilde ortaya konulmuş ve üç boyutlu çizimler ile ardiz bölgesinin gelişimi gösterilmeye çalışılmıştır.

CHAPTER 1. INTRODUCTION

1.1 An overview of the computational methods

In computational aerodynamics, the most important methods which are used to govern the aerodynamic flow regimes around complex configurations are semi-empirical and numerical methods [1].

The semi-empirical methods developed a variety of practical tools, not expensive in computer time, routinely used by the project engineering, but restricted to conventional configurations and global aerodynamics, (For a detailed description of semi-empirical methods see Ref.[1])

The numerical methods are essential methods to treat complicated configurations, to determine load distributions, local flow field properties, temperature distributions and to provide important insights into understanding complex flow mechanisms.

The numerical methods can be distinguished to four levels of equation from the most complex to less complex:

- Navier Stokes equation
- Euler equation
- Potential equation
- Linearized potential equation

In aerodynamics, the Reynolds-averaged **Navier-Stokes equations** model essentially all flow details. However, turbulence and transition needs to be modeled in a manner appropriate for the flow considered. The computer resources required for numerically solving the equations on a mesh that sufficiently resolves the boundary layers, free shear layers(wakes), vortex cores, etc. are still quite excessive.

For most high-Reynolds number flows of interest in aircraft aerodynamics viscous effects are confined to thin boundary layers, thin

wakes and centers of vortex cores, i.e. the global flow features depend only weakly on Reynolds number. This implies that a model based on **Euler's equations**, which allow the occurence of shock waves and convection of rotational flow, provides an appealing alternative. On a local scale, specifically at points where the flow leaves the surface (separates) and vorticity is shed into the flow field, some kind of model for viscous-flow dominated features will be required. Although the computer requirements of Euler codes can be met by the current generation of supercomputers, routine practical application of these codes (to simple configurations) is only just emerging.

If there are no strong shocks and if the rotational flow is confined to compact regions, the flow may be modeled as **potential flow** with embedded free vortex sheets and vortex cores. Now the rotational flow regions are "fitted" explicitly into the solution, rather than "captured" implicitly as part of the solution as is the case for above flow models. Although one has to decide a priori on the presence of vortex sheets and cores and generally the topology of the vortex system must be well-defined, "fitting" still requires that both the position and strength of the vortex sheets and cores have to be determined as a part of the potential-flow solution. The treatment of vortex sheets and vortex cores, freely floating in a fixed spatial grid, still poses considerable problems for finite difference/volume methods solving the nonlinear full potential codes are relatively modest, but application to general aircraft configurations is hampered by the grid-generation problem.

In case shockwaves are absent altogether and the perturbation on the free-stream due to the presence of the configuration is small, the potential-flow model is further simplified to the **linear potential flow** model, governed by the Prandtl-Glauert equation. (In incompressible flow the small perturbation assumption is not required and Laplace's equation applies.) Now the flow and the position of the vortex sheets and cores can be solved for by employing a boundary-integral type of approach utilizing singularity distributions exclusively on the surface of the configuration and the vortex sheets, not requiring a spatial grid. This linear potential flow model is the model underlying the classical panel method. It is emphasized at this point that though the governing equation is linear, the problem is still nonlinear because the position of the vortex sheets

appears nonlinearly in the boundary condition on the solid surface as well as in the boundary conditions on the vortex sheet itself. It can be argued that for most configurations in cruise condition the wakes remain fairly simple, i.e. do not roll up within one wing span downstream of the wing trailing edge. This leads to the conventional attached flow model in which the vortex sheets is chosen as some appropriate, user-specified rigid surface, rendering the resulting problem fully linear [2].

1.2 An overview of the computational methods on unsteady aerodynamics

In the course of developing computational methods to analyze complex aircraft maneuvers, the simulation of unsteady aerodynamics and the resulting wake dynamics is still an intriguing challenge. This time-dependent fluid dynamic modeling capability is much needed in aeronautical disciplines such as flight dynamics and flight simulation, and for time-dependent structural load analysis. Computation of a vehicle's stability derivatives, for example, at the first stages of shape development will then allow early flight simulation and evaluation of flying qualities. This capability will also result in benefits at the more advanced phases of prototype testing where experimental derivation of these stability derivatives is still limited and costly. Models of vortex wake motion can contribute too, to the investigation of leading-edge flow separation from swept wings, as would occur during high angle-of-attack landings or maneuvering of high speed vehicles. Similarly, estimation of rotorcraft vortex wake position can shed light on some of the more complex problems associated with a helicopter's flight [3].

Detailed solution of the complete nonlinear fluid dynamic equations along time-dependent flight paths is still in its initial phases [4]. The expansion of the computational grid to encompass large wake histories along curved, arbitrary path coordinates will only complicate the computation and make it more costly. An alternative approach postulates the use of simplified fluid dynamic equations while retaining the three-dimensional nature of both an aircraft geometry and its flight path. Such simplified fluid dynamic solutions were developed during the past years for inviscid steady flows[5], and were successful in simulating high Reynolds number, lifting, nonseparated, subsonic or supersonic flows.

1.3 Introduction to the wake analysis

In recent years, accurate analysis and reliable prediction of vortex flows become extremely important to aerodynamicists dealing with modern designs of fighter aircrafts, missiles and helicopters[6,7,8,9]. Modern fighter aircrafts fly at high angles of attack during take-off, offensive and defensive maneuvering, approach and landing. In this range of angle of attack, vortex flows develop around the aircraft with dominant effects on its aerodynamic characteristics and controllability. Modern designs of missiles require high launch angles of attack and high maneuverability within which a very complex vortex flow develops. For helicopters, the interaction of a blade with the vortex wake of another blade affects its operating performance, vibration and noise characteristics. In forward speeds, blade slap, a predominant source of external noise, occurs due to the rapid time rates of change of the blade pressure developing from its passage through a tip vortex of a preceding blade[10].

For all these applications, one has to deal with strong nonlinear aerodynamics. Compressibilty and separation of the flow are the main sources of the strong nonlinear effects. As the flow Mach number changes from low subsonic to transonic and supersonic, the flow undergoes several qualitative changes and shock waves (detached or attached) appear in the flow. As the angle of attack increases from low to moderate and high values, the lift- and pitching-moment coefficients become nonlinear functions of the angle of attack. This nonlinear behavior of the total loads is attributed to flow separations, from the wing edges (side and leading edges) and the body leeward side, in the form of vortex sheets that roll up into strong vortex cores[11].

Prediction of the coupled effects of nonlinearities; compressible and separated flow nonlinearities, is currently receiving considerable efforts from researchers working in the computational fluid dynamics (CFD) area, but it is far from being complete. In the supersonic flow regime, a few successful attempts based on the finite difference solution of Euler's equations exists. In the transonic flow regime, nothing is available yet and several efforts have just started[12,13].

1.4 Introduction to the present code

The lifting characteristics and wake structure of highly swept back and delta wings with sharp leading edges have lately attracted increased interest. This is partially due to the the desirable performance characteristics of those wings both at high supersonic cruise and at low subsonic short takeoff and landing conditions. The low-speed, high-lift condition is obtained with the aid of two strong vortices which emanate from the sharp leading edges of the wing. During certain low-speed maneuvers these leading-edge vortices might move and interact with the aircraft control surfaces, causing nonlinear stability derivatives. Analytical studies based on nonsteady aerodynamics of these conditions are still very limited, but this approach can significantly increase the understanding of some critical flight conditions (e.g., departure or stall spins).

Lifting surface methods based on steady aerodynamics for the calculation of leading-edge separated flows are now fairly well developed and are capable of solving the flow about complex geometries such as wing canard combinations. Johnson and Tinoco's[14] study is based on the experience of the Boeing Company that developed its own code. Also Lamar and Luckring[15] provides both experimental and theoretical data on configurations utilizing vortex flows. The major disadvantage of these style codes is the large amount of computer time required for complex wake geometries, since the final bound vorticity and wake rollup is obtained by an iterative technique. Moreover, the first assumed vortex wake shape which starts the iterative procedure should be close to the final solution to eliminate a possible convergence to an undesirable solution. Most of the current iterative methods report that the first guess for the vortex wake does not effect the final solution, but may increase substantially the computation time.

A time-dependent wing-following, wake-shedding procedure can provide both transient and asymptotic wake shapes and wing loadings without utilizing the iterative method. A similar method was developed by Djojodihardjo and Widnall [16] and was used later by Summa to solve complex wake shapes behind impulsively started helicopter rotors and wings[17]. These codes allow vortex rollup from side edges and wing tips but not leading-edge separation.

A study of the unsteady aerodynamic loads with allowance for leading-edge separation was reported by Atta et al.[18] and Kandil et al.[19]. They performed calculations for several nonsteady motions such as constant rolling and pitching oscillation and developed a special triangular leading-edge panel to allow leading-edge separation. An important feature of their model is the calculation of the pressure distribution about the wing with the local velocity distribution; that is, both forces and downwash for the boundary condition were calculated at the collocation points while other methods utilize the quarter panel vortex location for force calculation and the three-quarter panel collocation point for the boundary condition. However, the nonsteady vortex rollup was calculated by a complex iterative method, and the inclusion of the velocity potential derivatives in the Bernoulli equation is not reported clearly.

And finally, Katz formulated the nonsymettric motion of a slender delta wingvia Vortex Lattice method including tip and leading edge separations[20,21]. He performed calculations of the aerodynamic forces and time dependent wake rollup with non-iterative technique. However, he assumed that flow is incompressible and irrotational.

In the present thesis, a new doublet-lattice technique was developed for calculating the steady and unsteady flow about a three dimensional thin wing, with or without leading edge separation. Both leading-edge and trailing-edge wake rollup are determined numerically by a time-dependent vortex shedding procedure that does not require an iterative technique as do most present steady-state solutions. This considerably reduces the computational effort since the final number of wake elements is obtained only at the latest time step. Furthermore, the present method can provide transient aerodynamic loads and wake geometries during the time-dependent motion and improves the understanding of some vortex interaction problems.

CHAPTER 2. FUNDAMENTAL THEORY

2.1 Governing equation and boundary conditions

Methods such as doublet lattice or vortex lattice are widely used for calculating the pressure distribution about lifting surfaces in steady and oscillatory potential flows along a straight flight path. These methods can be modified further to solve the time-dependent lift variations on the wings of a maneuvering aircraft. While extending the steady-state lifting surface model for the calculation of nonsteady flight along a curved path, the following corrections have to be made:

1) Correction of downwash distribution on wing surface via a transformation which enables the statement and linearization of the nonsteady boundary condition of zero flow assumption across the wing surface.

2) A modification in the pressure distribution term must be made, since the Bernoulli equation includes additional nonsteady effects.

3) A nonsteady wake model must be constructed, which releases vortex ring elements from the trailing edge as the planform circulation varies. The strength of each element must satisfy Kelvin's theorem of no net circulation generation. An additional improvement that is strongly recommended is the calculation of wake distortion in the wing-wake -induced velocity field. This calculation can provide valuable information about vortex wake shape and location behind the aircraft.

Modifications 1 and 2 are carried out by solving the problem in a non-inertial frame of reference that follows the wing in such a way that its x direction is always tangent to the flight path. The orthogonal displacement in this system is limited to small displacements. However, the path curvature should be such that the flow disturbances caused by the wing should remain small.

Lattice methods as well as the present method assume that viscous

effects can be accounted for by proper modeling of the flow. That implies that information such as the location of separation lines and strength of the shed vorticity is to be supplied by an experiment, flow visualization, or viscous flow calculations. When such information is provided to the potential flow model, the wake rollup and pressure distribution about the wing can be calculated. Air considered to be an ideal gas. Viscosity and heat conduction are negligible. The basic assumption of such a model is that flow is isentropic, irrotational, and homogeneous over the whole fluid region excluding the wing and its wake. The difference of this method from the other lattice methods is the compressibility effect. The flow is compressible and includes only subsonic region.

With the above definition the continuity equation in a stationary inertial co-ordinate system (x^*, z^*) (see Fig. 1) is

$$\nabla^2 \phi^* = 0 \tag{2.1}$$

where ϕ^* is the time-dependent velocity potential due to the wing motion and its wake. This potential can be separated into the plate disturbance potential ϕ_0^* and the wake potential ϕ_w^*, assumed to consist of distributed vortices situated on a deforming sheet (see Fig. 2):

$$\phi(x^*, z^*, t^*) = \phi_0^* + \phi_w^* \equiv \phi^* \tag{2.2}$$

The boundary conditions for Eq. (2.1) are as follows.

(a) There is no flow through the wing surface $z^* = h(x^*, t^*)$:

$$\partial\phi^*/\partial z^* \big|_{\text{on wing}} = \partial\phi^*/\partial x^* \cdot \partial h(x^*, t^*)/\partial x^* + \partial h(x^*, t^*)/\partial t^* \tag{2.3.a}$$

(b) The disturbance decays far from the wing surface:

$$\nabla\phi^* \to 0 \text{ as } |x^*|, |y^*|, |z^*| \to \infty. \tag{2.3.b}$$

Furthermore, for the nonsteady flow, some kind of angular momentum conservation is required, i.e., the overall circulation Γ generated in the fluid must be zero (Kelvin's condition)

$$d\Gamma/dt = 0 \quad (\text{ for all } t) \tag{2.4}$$

To obtain a unique solution of the wing circulation [through Eqs. (2.1-2.4)] a smooth tangential flow at the trailing edge is also assumed. This condition is known as the Kutta condition, which requires finite velocities at the trailing edge. In terms of the velocity potential ϕ this condition can be imposed via the formulation

$$\nabla\phi < \infty \quad (\text{ at the trailing edge }) \tag{2.5}$$

The instantaneous pressure P at each point on the wing is calculated from Bernoulli's equation:

$$(P_\infty - P)/\rho = -1/2\left[(\partial\phi^*/\partial x^*)^2 + (\partial\phi^*/\partial z^*)^2\right] + \partial\phi^*/\partial t^* \tag{2.6}$$

The solution of the boundary-value problem (2.1)-(2.4) is very complicated owing to the wing surface condition (2.3). This difficulty is overcome by transforming the problem, which has been stated in the inertial frame of reference (x*,z*), into a system (x,z), where the boundary condition on the wing surface is more easily stated. This transformation is

$$x = \cos[\theta(t)].[x^* - S_x*(t)] + \sin[\theta(t)].[z^* - S_z*(t)],$$
$$z = -\sin[\theta(t)].[x^* - S_x*(t)] + \cos[\theta(t)].[z^* - S_z*(t)], \tag{2.7}$$
$$t = t^*,$$

where θ is the inclination of the (x,z) co-ordinate system relative to the (x*,z*) frame and (S_x*, S_z*) are the path components (Fig. 2). The transformed continuity equation is

$$\nabla^2\phi = 0,$$

$$\phi(x, z, t) = \phi_0 + \phi_w \equiv \phi \tag{2.8}$$

The potential ϕ is defined only in the inertial (x^*, z^*) system because definition of a non-rotational velocity potential in the rotating frame (x,z) is impossible. Therefore the derivatives $\partial\phi/\partial x$ and $\partial\phi/\partial z$ are the velocities parallel to the x and z directions as measured in the (x^*, z^*) system.

The transformed boundary conditions are

$$\partial\phi_0/\partial z|_{z=0} = [\, U(t) + \partial\phi/\partial x].\partial h(x,t)/\partial x + \partial h(x,t)/\partial t - \partial\phi_w/\partial z + \omega x \equiv W_{ij} \qquad (2.9)$$

where ω is the time-dependent angular velocity vector of the (x,z) frame, also

$$\nabla\phi_0 \to 0 \text{ as } |x|, |y|, |z| \to \infty,$$

$$(P_\infty - P)/r = \{[z.\omega + U(t)]\partial/\partial x - x.\omega.\partial/\partial z + \partial/\partial t\}\phi - 1/2[(\partial\phi/\partial x)^2 + (\partial\phi/\partial z)^2]$$

$$(2.10)$$

According to Katz [22] the crossed-out terms can be neglected, since the velocity perturbations are small compared to the freestream velocity [$U(t) >> \partial\phi/\partial x, \partial\phi/\partial y, \partial\phi/\partial z$]. Furthermore, in Eq. (2.10) the terms containing the angular velocities also can be neglected, as their contribution to the pressure difference across the wing is symmetrical. The general solution of Eq. (2.1) is a sum of doublet and source distributions on the wing geometry and doublet distributions on the wake region.

In order to solve the potential ϕ, its derivative with respect to z (while $z \to 0$) is compared to the downwash in boundary condition, Eq. (2.9):

$$W_{ij} = -[\, (U(t) - r.y)(\partial h/\partial x - \sin\alpha_i) - q.x + p.y + \partial h/\partial t\,] \qquad (2.11)$$

where $U = U(t)$ and $z = h(x, y, t)$ are the momentary flight velocity and

orthogonal wing displacement, respectively, while (p, q, r) are the angular velocity components. Also α_i is the attack angle of each panel.

2.2 Method of solution

Before describing the method it will be beneficial to lay some groundwork on the basic building blocks used in this method. The method is based on the classic subsonic source shown in Fig. 3 (m = 1). More actually speaking this method uses velocity and pressure doublets (double sources) which can be derived from the classic subsonic source.

Fig. 4 shows graphically how two sources (source and a sink) are combined into a double-source and how, in the limit, the result is a doublet. Lines with arrows indicate streamlines. Lines without arrows indicate lines of constant potential. There is a jump in potential across the doublet point. The double-source or doublet strength, $\Delta\phi$, is equal to the limit of $\sigma\Delta N$ as ΔN goes to zero and σ goes to infinity. Source flow is radial, outward (source) or, inward (sink). The velocity doublet acts like· a pump sucking fluid in one side and pushing it out the other. The implications of placing a distribution of such doublets on a surface is shown in the next figure.

Fig. 5 illustrates the equivalence between doublet distributions and vortex lines for two simple but practical examples. A derivation of this eqivalence for the general case of variable doublet strength placed on an arbitrary surface is given in Ref. [23]. The horseshoe vortex shown in this figure is a very practical aerodynamic device which is used in both the Vortex and Doublet Lattice Methods. It also is equivalent to the pressure doublet, shown in Fig. 6, for the steady case (as the width of the horseshoe vortex becomes small, i.e., a doublet line extending from the doublet origin to downstream infinity).

The basic concepts associated with the pressure doublet are illustrated in Fig. 4. The pressure doublet comes from a linear combination the space (x) and time derivative of the potential. Since these derivatives satisfy the basic differential equation so does a linear combination of such variables. If a linear form of the pressure equation is used, then C_p itself satisfies the basic differential equation. An expression for a pressure doublet

can then be written analogous to the potential doublet where C_p replaces ϕ and ΔC_p replaces $\Delta \phi$. Fig. 4 presents an outline of this process.

In Fig. 4 the lines of constant ϕ are shown for a potential doublet. Fig. 6 shows the same pattern for lines of constant C_p. The pressure doublet is considered to be a very convenient aerodynamic device to use in solving lifting surface problems since it is caused by a pressure differential, ΔC_p, across the lifting surface. Since there is no pressure discontinuity in the wake of a lifting surface, $\Delta C_p = 0$, only the lifting surface must be considered when using the pressure doublet. It has been said that it is more convenient to use than methods that treat the wake separately and explicitly.

The general solution of Eqs. (2.1-2.4), according to Green's theorem[24], consists of a doublet and source distribution over the wing surface. However, for the lifting problem solution, the vortex distribution, which is derived from the doublets, is sufficient. It has been shown in Ref. [25] that the velocity induced by a doublet distribution can be expressed as the velocity induced by a vorticity distribution plus the velocity induced by a concentrated vortex along the boundary of the distribution. Furthermore it has been shown in the same reference that the components of the velocity induced by a vorticity distribution can be expressed in terms of the components of the velocity induced by a source distribution. It is therefore sufficient to evaluate the integrals associated with the velocity induced by a source distribution on a wing panel and by the concentrated vortices along the edges of a wing panel and by the concentrated vortices along the edges of a wake panel.

To obtain the velocity induced by the source distribution on the configuration in subsonic and supersonic flow the same procedure is followed as in Ref. [26]. In this procedure the components of the velocity induced in subsonic and supersonic flow are obtained from those induced in incompressible flow by applying the Gothert transformation and a generalized Gothert transformation respectively. Thus as far as the evaluation of the integrals in the velocity induced by source distributions is concerned it suffices to consider the velocity induced by these distributions in incompressible flow.

Therefore, the wing planform of Fig. 7 was divided into panels as shown in Fig. 8, and at each panel a vortex ring and a source was placed. Also a collocation point [where boundary condition (2.3) is fulfilled] is placed at the panel center. By selecting the vortex ring representation, which is a partial solution of Eqs. (2.1-2.3) the Kelvin condition is also fulfilled [Eq. (2.4)]. In addition, the separated vortex strength Γ_{li} is adjustable to simulate various leading-edge radii. In this study, however, sharp leading edges were assumed; consequently, the leading edge separated vortex strength was set equal to the corresponding triangular panel strength Γ_{li}.

The extension of this model, in order to construct a three-dimensional vortex-panel element, was found to be sufficient to satisfy Eq. (2.5). Then for the complete solution of the problem, in terms of the unknown bound vortices Γ_{bi}, only boundary condition (2.3) is left to be solved; i.e., the induced velocity $(\partial\phi/\partial z)_{ij}$ due to the wing vortices and its trailing edge wake elements Γ_{ti} and leading edge wake elements Γ_{li} is given at each collocation point by,

$$(\partial\phi/\partial z)_{ij} = [\,A_{bij}\,]\begin{vmatrix}\vdots\\\Gamma_{bi}\\\vdots\\i=n\end{vmatrix} + [\,A_{tij}\,]\begin{vmatrix}\vdots\\\Gamma_{ti}\\\vdots\\i=l\end{vmatrix} + [\,A_{lij}\,]\begin{vmatrix}\vdots\\\Gamma_{li}\\\vdots\\i=m\end{vmatrix} \qquad (2.12)$$

the first term on the right, $[A_b]$ stands for all the influence coefficients resulting from the Biot Savart bound vortex influence calculations. The second and third terms $[A_t]$ and $[A_l]$ represents the influence coefficients of the trailing-edge wake Γ_{ti} and leading-edge separated elements Γ_{li}, and their strength is known from previous time steps.

In order to fulfill Eq.(2.3) the sum of the velocities relative to the panel must be zero,

$$w_{ij} + (\partial\phi/\partial z)_{ij} = 0 \qquad (2.13)$$

and by substituting Eqs.(2.11) and (2.12) into Eq.(2.13),

$$\left(U - r \cdot y_i\right)\left(\frac{\partial h}{\partial x} - \sin\alpha_i\right) - q \cdot x_i + p \cdot y_i + \frac{\partial h}{\partial t}$$

$$= \left[A_b\right] \cdot \begin{vmatrix} \cdot \\ \Gamma_b \\ \cdot \\ i = n \end{vmatrix} + \left[A_t\right] \cdot \begin{vmatrix} \cdot \\ \Gamma_t \\ \cdot \\ i = m \end{vmatrix} + \left[A_l\right] \cdot \begin{vmatrix} \cdot \\ \Gamma_l \\ \cdot \\ i = l \end{vmatrix} \tag{2.14}$$

2.3 Determination of aerodynamic influence coefficients

Three types of aerodynamic influence coefficients can be distinguished, namely:

    i) the coefficients associated with the influence of source distributions on a wing panel

    ii) the coefficients associated with the influence of doublet distributions on a wing panel

    iii) the coefficients associated with the influence of doublet distributions on a wake panel.

The velocity components induced by the wing source distribution, which have two contributions one from "leading edge" and the other from "trailing edge" source distributions, are

$$\vec{b}_{w_i} = \vec{U}_{sl_{i-1}} + \vec{U}_{st_i} \tag{2.15.a}$$

with

$$\vec{U}_{sl_i} = \frac{1}{4\pi} \int_{y_j}^{y_{j+1}} d\eta \int_{x_{le}^i(\eta)}^{x_{le}^i(\eta)} q_l^i(\xi,\eta) \frac{\vec{r}}{|\vec{r}|^3} d\xi \tag{2.15.b}$$

and

$$\vec{U}_{st_i} = \frac{1}{4\pi} \int_{y_j}^{y_{j+1}} d\eta \int_{x_{le}^i(\eta)}^{x_{le}^i(\eta)} q_t^i(\xi,\eta) \frac{\vec{r}}{|\vec{r}|^3} d\xi \tag{2.15.c}$$

The velocity components induced by the wing or wake doublet distribution are the sum of vorticity distribution of the panel and edge vortices along the inboard and outboard edges of the panel.

The first component is obtained from the correspondence relation

between source and vorticity distributions. The velocity components induced by a constant wing source distribution are given by,

$$\vec{U}_{sc_i} = \frac{1}{4\pi} \int_{y_j}^{y_{j+1}} d\eta \int_{x_{le}^i(\eta)}^{x_{te}^i(\eta)} \frac{\vec{r}}{|\vec{r}|^3} d\xi \tag{2.16}$$

Now, the wing vorticity distribution can be written as the sum of "leading edge" and "trailing edge" contributions as

$$\vec{a}_{wp_i} = \vec{U}_{dlp_i} + \vec{U}_{dtp_i} \tag{2.17.a}$$

with

$$\vec{U}_{dlp_i} = \vec{U}_{sl_i} (\vec{e}_z, -y_{i-1}\vec{e}_z, y_{i-1}\vec{e}_y - \vec{e}_x) \tag{2.17.b}$$

$$\vec{U}_{dtp_i} = -\vec{U}_{dlp_{i+1}} + \vec{U}_{sc_i} \cdot (\vec{e}_z, -y_i\vec{e}_z, y_i\vec{e}_y - \vec{e}_x) \tag{2.17.c}$$

where e_x, e_y, e_z are the unit vectors in x, y and z, respectively.

The second component can be written in similar terms as done in the first contribution,

$$\vec{a}_{we_i} = \vec{U}_{dle_{i-1}} + \vec{U}_{dte_i} \tag{2.18.a}$$

with

$$\vec{U}_{dle_i} = \frac{1}{4\pi} (\vec{e}_x \times \vec{R}_j) \int_{x_i}^{x_{i+1}} \Gamma_{in_l}^i(\xi) \frac{d\xi}{|R_j|^3}$$
$$- \frac{1}{4\pi} (\vec{e}_x \times \vec{R}_{j+1}) \int_{x_{le}}^{x_{te}} \Gamma_{out_l}^i(\xi) \frac{d\xi}{|R_{j+1}|^3} \tag{2.18.b}$$

$$\vec{U}_{dte_i} = \frac{1}{4\pi} (\vec{e}_x \times \vec{R}_j) \cdot \int_{x_i}^{x_{i+1}} \Gamma_{in_t}^i(\xi) \frac{d\xi}{|R_j|^3}$$
$$- \frac{1}{4\pi} (\vec{e}_x \times \vec{R}_{j+1}) \cdot \int_{x_{le}}^{x_{te}} \Gamma_{out_t}^i(\xi) \frac{d\xi}{|R_{j+1}|^3} \tag{2.18.c}$$

where $R_k = (x_0 - \xi, y_0 - y_k, z_0)$.

2.4 Evaluation of the integrals of aerodynamic influence coefficients

In section (2.3), the aerodynamic influence coefficients are written in integral form. The solution of these integrals are shown in Ref. [26]. In this section, solution of these integrals are given for incompressible flow

and for subsonic flow according to Ref. [25]. Essentially, the integrals are solved for incompressible flow and the resulting expressions for subsonic flow are computed through the application of Gothert transformation.

2.4.1 Incompressible flow

2.4.1.1. Source distribution on a wing panel

The velocity components of the source distribution on a wing panel which have two different contributions are given in the wing panel coordinate system, Fig. 9. The contributions from the "leading edge" distributions are

$$U_{sl_i}^k = \frac{1}{4\pi A_i}\left[-zF_1^k - (b_1 - \nu_k b_k \frac{\nu_1 - \nu_k}{1+\nu_k^2})G_1^k - (y-y_k)G_2^k + \frac{\nu_k - \nu_1}{1+\nu_k^2}G_3^k\right]$$

$$V_{sl_i}^k = \frac{1}{4\pi A_i}\left[\nu_1 \cdot zF_1^k + (b_1\nu_k - b_k \frac{\nu_1 - \nu_k}{1+\nu_k^2})G_1^k - b_1 G_2^k + \frac{1+\nu_1 \cdot \nu_k}{1+\nu_k^2}\cdot G_3^k\right]$$

$$W_{sl_i}^k = \frac{1}{4\pi A_i}\left[-b_1 F_1^k + z(1+\nu_1\nu_k)G_1^k - \nu_1 z G_2^k\right], \quad k=1,2,3,4 \qquad (2.19)$$

The contributions from the "trailing edge" distribution are

$$U_{st_i}^k = \frac{1}{4\pi A_i}\left[zF_1^k + (b_2 - \nu_k b_k \frac{\nu_2 - \nu_k}{1+\nu_k^2})G_1^k + (y-y_k)G_2^k + \frac{\nu_2 - \nu_k}{1+\nu_k^2}\cdot G_3^k\right]$$

$$V_{st_i}^k = \frac{1}{4\pi A_i}\left[-\nu_2 zF_1^k - (b_2\nu_k + b_k\frac{\nu_2 - \nu_k}{1+\nu_k^2})G_1^k + b_2 G_2^k - \frac{1+\nu_2\nu_k}{1+\nu_k^2}\cdot G_3^k\right]$$

$$W_{st_i}^k = \frac{1}{4\pi A_i}\left[+b_2\cdot F_1^k - z(1+\nu_2\nu_k)G_1^k + \nu_2 z\cdot G_2^k\right], \quad k=1,2,3,4 \qquad (2.20)$$

The velocity induced by a constant wing source distribution is

$$U_{sc_i}^k = -\left(\tfrac{1}{4\pi}\right)\cdot G_1^k$$

$$V_{sc_i}^k = \left(\tfrac{1}{4\pi}\right)\cdot\left(-G_2^k + \nu_k\cdot G_1^k\right)$$

$$W_{sc_i}^k = -\left(\tfrac{1}{4\pi}\right)\cdot F_1^k \qquad , \quad k=1,2,3,4 \qquad (2.21)$$

where the elementary functions F^1_k, G^1_k, G^2_k, G^3_k and b_k are

$$F_1^k = -\tan^{-1}\frac{Z(X^2+Y^2+Z^2)}{\gamma_k Z^2 - Y \cdot b_k} + \frac{\pi}{2}$$

$$G_1^k = \frac{1}{(1+\gamma_k^2)^{1/2}} \cdot \sinh^{-1}\frac{Y+\gamma_k \cdot X}{(b_k^2 + (1+\gamma_k^2)\cdot Z^2)^{1/2}}$$

$$G_2^k = \sinh^{-1}\frac{X}{(Y^2+Z^2)^{1/2}}$$

$$G_3^k = (X^2+Y^2+Z^2)^{1/2}$$

$$b_k = X - \gamma_k \cdot Y \quad , \quad X = x - x_k \quad , \quad Y = y - y_k \quad , \quad Z = z \tag{2.22}$$

2.4.1.2. Doublet distributions on a (wing and/or wake) panel

The velocity components induced by the doublet distributions, see Fig. 10, are divided into two distributions one from vorticity distribution, and the other from concentrated edge vortices. Each of them has two contributions from leading and trailing edges on a panel.

The velocity components induced by the panel vorticity distribution are given in Equation (2.18). The "leading edge" contributions of the panel concentrated edge vortices are

$$U_{dle_i}^k = 0$$

$$V_{dle_i}^k = \frac{z}{8\pi A_i}\left[G_2^k + \frac{x-x_k}{(y-y_k)^2+z^2}\cdot G_3^k\right]$$

$$W_{dle_i}^k = -\frac{(y-y_k)}{z}\cdot V_{dle_i}^k \tag{2.23}$$

The "trailing edge" contributions of the panel concentrated edge vortices are

$$U_{dte_i}^k = 0$$

$$V_{dte_i}^k = -V_{dle_i}^k + \frac{z}{4\pi}\left[\frac{1}{(y-y_k)^2+z^2}\cdot G_3^k\right]$$

$$W_{dte_i}^k = -\frac{(y-y_k)}{z}\cdot V_{dte_i}^k$$

$$\tag{2.24}$$

2.4.2. Subsonic Flow

The components of the velocity derived in section (2.4.1.) are in local coordinate system of each panel. To calculate the velocity components in subsonic flow, the Gothert transformation should be applied.

2.4.2.1. Source distribution on a wing panel

The "leading edge" contributions from wing source distribution are

$$U_{sl_i}^k = \frac{K}{4\pi A_i}\left[zF_{1c}^k - \left(b_1 - y_k b_k \cdot \frac{y_k - y_1}{-\beta^2 - y_k^2}\right)G_{1c}^k - (y - y_k)G_{2c}^k - \frac{y_k - y_1}{-\beta^2 - y_k^2}G_{3c}^k\right]$$

$$V_{sl_i}^k = \frac{K}{4\pi A_i}\left[-y_1 z F_{1c}^k + \left(b_1 y_k + \beta^2 \cdot b_k \frac{y_k - y_1}{-\beta^2 - y_k^2}\right)G_{1c}^k - b_1 \cdot G_{2c}^k + \frac{-\beta^2 - y_1 y_k}{-\beta^2 - y_k^2} \cdot G_{3c}^k\right]$$

$$W_{sl_i}^k = \frac{K}{4\pi A_i}\left[b_1 F_{1c}^k - z(-\beta^2 - y_1 \cdot y_k)G_{1c}^k - y_1 \cdot z \cdot G_{2c}^k\right] \quad, \quad k = 1,2,3,4 \quad (2.25)$$

The "trailing edge" contributions from wing source distribution are

$$U_{st_i}^k = \frac{K}{4\pi A_i}\left[-zF_{1c}^k + \left(b_2 - b_k y_k \frac{y_k - y_2}{-\beta^2 - y_k^2}\right)G_{1c}^k - (y - y_k)G_{2c}^k + \frac{y_k - y_2}{-\beta^2 - y_k^2}G_{3c}^k\right]$$

$$V_{st_i}^k = \frac{K}{4\pi A_i}\left[y_2 z \cdot F_{1c}^k - \left(b_2 y_k + \beta^2 b_k \frac{y_k - y_2}{-\beta^2 - y_k^2}\right)G_{1c}^k + b_2 G_{2c}^k - \frac{-\beta^2 - y_k^2}{-\beta^2 - y_2 y_k} \cdot G_{3c}^k\right]$$

$$W_{st_i}^k = \frac{K}{4\pi A_i}\left[-b_2 F_{1c}^k + z(-\beta^2 - y_2 \cdot y_k)G_{1c}^k + y_2 \cdot z \, G_{2c}^k\right] \quad, \quad k = 1,2,3,4 \quad (2.26)$$

the constant source distribution on the panel is

$$U_{sc_i}^k = -\left(\frac{K}{4\pi}\right) \cdot G_{1c}^k$$

$$V_{sc_i}^k = \left(\frac{K}{4\pi}\right) \cdot \left(-G_{2c}^k + y_k \cdot G_{1c}^k\right)$$

$$W_{sc_i}^k = \left(\frac{K}{4\pi}\right) \cdot F_{1c}^k \quad\quad, \quad k = 1,2,3,4$$

$$(2.27)$$

where the elementary functions F_{1c}^k, G_{1c}^k, G_{2c}^k, G_{3c}^k and b_k are defined as

$$F_{1c}^{k} = \tan^{-1} \frac{z(x^2 + \beta^2(Y^2 + Z^2))^{\frac{1}{2}}}{\nu_k \cdot (Y^2 + Z^2) - X.Y}$$

$$G_{1c}^{k} = \frac{1}{(\beta^2 + \nu_k^2)^{\frac{1}{2}}} \cdot \sinh^{-1} \frac{\beta^2 Y + \nu_k . X}{\beta(b_k^2 + (\beta^2 + \nu_k^2).Z^2))^{\frac{1}{2}}}$$

$$G_{2c}^{k} = \sinh^{-1} \frac{X}{\beta(Y^2 + Z^2)^{\frac{1}{2}}}$$

$$G_{3c}^{k} = (X^2 + \beta^2(Y^2 + Z^2))^{\frac{1}{2}}$$

with

$$b_k = X - \nu_k . Y$$

$$X = x - x_k \quad , \quad Y = y - y_k \quad , \quad Z = z \quad , \quad k = 1,2,3,4 \tag{2.28}$$

2.4.2.2. Doublet distributions on a (wing and/or wake) panel

The "leading edge" contributions of the vorticity distribution on the panel are

$$U_{dlp_i}^{k} = W_{sl_i}^{k}$$

$$V_{dlp_i}^{k} = -\nu_1 . W_{sl_i}^{k}$$

$$W_{dlp_i}^{k} = \nu_1 . V_{sl_i}^{k} - \beta^2 U_{sl_i}^{k} \quad , \quad k = 1,2,3,4 \tag{2.29}$$

The "trailing edge" contributions of the vorticity distribution on the panel are

$$U_{dtp_i}^{k} = -U_{dlp_i}^{k} + W_{sc_i}^{k}$$

$$V_{dtp_i}^{k} = -V_{dlp_i}^{k} - \nu_1 . W_{sc_i}^{k}$$

$$W_{dtp_i}^{k} = -W_{dlp_i}^{k} + \nu_1 . V_{sc_i}^{k} - \beta^2 . U_{sc_i}^{k} \quad , \quad k = 1,2,3,4 \tag{2.30}$$

The "leading edge" contributions of the concentrated edge vortices on the each panel are

$$U^k_{dle_i} = 0$$

$$V^k_{dle_i} = \frac{z \cdot K}{8\pi A_i}\left[\beta^2 \cdot G^k_{2c} + \frac{x-x_k}{(y-y_k)^2+z^2} G^k_{3c}\right]$$

$$W^k_{dle_i} = -\frac{(y-y_k)}{z} \cdot V^k_{dle_i} \quad , \quad k=1,2,3,4 \tag{2.31}$$

The "trailing edge" contributions of the concentrated edge vortices on the each panel are

$$U^k_{dte_i} = 0$$

$$V^k_{dte_i} = -V^k_{dle_i} + \frac{zK}{4\pi}\left[\frac{1}{(y-y_k^2)+z^2} G^k_{3c}\right]$$

$$W^k_{dte_i} = -\frac{(y-y_k)}{z} \cdot V^k_{dte_i} \quad , \quad k=1,2,3,4 \tag{2.32}$$

2.5 Calculational procedure of the system of equations

In order to deal with the arbitrary nonsteady motion of a wing, and to enable the study of wake distortion, a detailed wake model was constructed[27]. The wake and wing circulations must fulfill Kelvin's law (Eq. 2.4) for each time step; i.e., the overall circulation generated in the flow must be zero, otherwise, the model will consist of closed vortex rings. At each time step, when the solution of the wing circulation (or potential) is solved, the wake elements are allowed to deform in the wing-wake-induced velocity field.

The application of steady wing theory solutions to the nonsteady flight problems in curved flight involves three major modifications. The first two are the wing surface downwash correction and a more detailed wake model, while third change results from additional $\partial\phi/\partial t$ term in Eq. (2.6).

As previously stated, in Eq.(2.14), (p,q,r) is the rotational motion around the (x,y,z) axes correspondingly, U(t) is the momentary far-field velocity, and a_i is the panel angle of attack. The heaving motion of the panel relative to the (x,y,z) axes is $h_i(t)$, and its effect on the downwash

is the $\partial h_i/\partial t$ term. The first term on the right, [A_b], stands for all the influence coefficients resulting from the Biot Savart bound vortex influence calculations. The second and third terms [A_t] and [A_l] represents the influence coefficients of the trailing-edge wake Γ_{ti} and leading-edge separated elements Γ_{li}, and their strength is known from previous time steps.

Eq. (2.14) is derived for all n panels on their collocation points resulting in n equations with n unknown Γ_{bi} at each time interval. If wing shape is not varying during flight (flap motion ailerons, etc.) the coefficients A_{bij} are constant and their calculation is performed only once. The calculational effort of A_{lij} and A_{tij} increases with time as the number of wake elements grows. This must be performed at each time interval since wake rollup changes the geometry involved in its induced velocity calculations.

To demonstrate the calculation procedure it is assumed that at $t=0$ the wing was set suddenly into motion. The first calculation takes place at $t=t_0$ as it is shown in Fig. 10, and the spanwise wake vortex is placed in the midinterval traveled $(1/2U\Delta t)$. For the linear (not separated) transient calculation there is no direct coupling between the panel length a_p and the time step, but for more precise accuracy the nondimensional time step should be smaller than 0.2 $(\Delta tU/c < 0.2)$. For separated flow, however it is recommended that the time steps and panel lengths should be of the same order of magnitude $(\Delta tU/a_p \cong 1)$ to prevent the separated wake elements from being too close to the wing collocation points [20].

After the first time step the momentary position and angular motion of the wing are known and the geometrical boundary condition for the downwash [left side of Eq. (2.14)] is determined. Then the influence coefficients [A_{bij}] are calculated while [A_{tij}]=[A_{lij}]=0 for the first time step, since there is no free wake elements shed as yet.

$$
\left(U - r \cdot y_i\right)\left(\frac{\partial h}{\partial x} - \sin\alpha_i\right) - q \cdot x + p \cdot y + \frac{\partial h}{\partial t} = \left[A_b\right] \cdot \begin{vmatrix} \vdots \\ \Gamma_{b_i} \\ \vdots \\ i=n \end{vmatrix}
$$

(2.33)

Solution of the above equation is required the evaluation of the aerodynamic influence coefficients which are described in Section 2.4. Gauss elimination method is used by partial pivoting of coefficients for solving the unknown strengths of panel singularities. At this point the bound vorticity strength Γ_{bi} is solved and the wake rollup step is performed by moving the wake points shed at $t = t_0$.

2.6 Modelling of the vortex wake

The modelling of the vortex wake, which is shed at the wing leading and trailing edges, is performed by releasing vortex segments at each time interval Δt, see Fig. 11. As above calculations are completed the wake deformation is simulated by calculating the downwash at each vortex edge location $(u,v,w)_i$ in Eq. (2.34)

$$
(u,v,w)_i = [A_{bw}] \cdot \left| \Gamma_{b_i} \right|_{i=n} + [A_{tw}] \cdot \left| \Gamma_{t_i} \right|_{i=m} + [A_{lw}] \cdot \left| \Gamma_{l_i} \right|_{i=l}
$$

(2.34)

which is similar to the right hand side of Eq. (2.14), but here A_{bwij}, A_{twij}, and A_{lwij} are the influence coefficients relative to those vortex edges.

The solution algoritm of above equation same with Eq. (2.33) but here the wing and wake elements induced velocity to the wake elements edges. Here the separated leading edge wake, trailing edge wake, and wing vortex elements is l, m, and n, respectively.

The motion of the wake element points $(\Delta x, \Delta y, \Delta z)_i$ is then calculated by the use of Eq. (2.35),

$$
(\Delta x, \Delta y, \Delta z)_i = (u,v,w)_i \cdot \Delta t
$$

(2.35)

2.6 Calculation of aerodynamic coefficients

To conclude the calculation procedure for a given time step, the forces acting on the foil are determined by applying the nonsteady Bernoulli's equation as derived before. That is,

$$\frac{P_\infty - P}{\rho} = (U - ry)\cdot\frac{\partial\phi}{\partial x} + \frac{\partial\phi}{\partial t} + \frac{1}{2}\left[\left(\frac{\partial\phi}{\partial x}\right)^2 + \left(\frac{\partial\phi}{\partial y}\right)^2 + \left(\frac{\partial\phi}{\partial z}\right)^2\right]$$

(2.36)

By integrating the pressure along a given panel with length of $\Delta x_i = x_{i+1} - x_i$ and by neglecting smaller terms $[U(t) >> (\partial\phi/\partial x),(\partial\phi/\partial y),(\partial\phi/\partial z)]$ and assuming $r = 0$ for the present calculation, the following expression for the pressure difference ΔP_i across each panel can be derived:

$$\Delta P_i = \frac{2\rho}{\Delta s_i}\left[\left(U\int_{x_{i-1}}^{x_i}\frac{\partial\phi}{\partial x}dx\right)\Delta y_i + \left(V\int_{y_{i-1}}^{y_i}\frac{\partial\phi}{\partial y}dy\right)\Delta x_i \right.$$
$$\left. + \int_{x_{i-1}}^{x_i}\left(\frac{\partial}{\partial t}\int_{0}^{x}\frac{\partial\phi}{\partial x}dx\right)dx\,\Delta y_i\right]$$

(2.37)

also Eq. (2.37) can be rewritten for the normal force per unit width on the panel,

$$\Delta F_i = \Delta P_i \cdot \Delta s_i = 2\rho\left(U\int_{x_i}^{x_{i+1}}\frac{\partial\phi}{\partial x}dx + \int_{x_i}^{x_{i+1}}\frac{\partial}{\partial t}\int_{0}^{x}\frac{\partial\phi}{\partial x}dx\,dx\right)$$
$$\simeq \rho\left\{U\cdot\Gamma_b + \frac{\partial}{\partial t}\left[\left(\sum_{k=1}^{i}\Gamma_{b_k} + \sum_{k}^{i+1}\Gamma_{b_k}\right)\frac{\Delta x}{2}\right]\right\}$$

(2.38)

Here the summation

$$\sum_{k=1}^{i}\Gamma_{b_k}$$

is performed along the chordline only, starting at the leading edge panel ahead of the panel that its normal force ΔF_i is to be calculated. The momentary lift, drag, pitching moment, and rolling moment coefficients

(assuming no leading-edge suction for the separated flow) are obtained by integrating each panel normal force ΔF_i along the wing surface,

$$C_L = \sum_{i=1}^{n} \Delta F_i \cos\alpha_i \Big/ \frac{1}{2}\rho U^2 S \tag{2.39}$$

$$C_D = \sum_{i=1}^{n} \Delta F_i \cdot \sin\alpha_i \Big/ \frac{1}{2}\rho U^2 S \tag{2.40}$$

$$C_m = \sum_{i=1}^{n} \Delta F_i \cdot x_i \Big/ \frac{1}{2}\rho U^2 S \cdot c \tag{2.41}$$

$$C_\ell = \sum_{i=1}^{n} \Delta F_i \, y_i \Big/ \frac{1}{2}\rho U^2 S \cdot c \tag{2.42}$$

where S is the wing area, c is the chord and b is the span of the wing.

Once the above described calculation is completed, a time increment Dt is added and the wing is advanced to its new location. Then a vortex ring is shed both at the trailing-edge and leading-edge panels. The strength of the latest shed vortex ring is set equal to the shedding vortex strength at the previous time step. As the wake shedding process is completed, the bound vorticity is calculated by Eq. (2.14), the wake rollup performed with Eq. (2.35) and the forces and moments acting are indicated by Eqs. (2.39), (2.40), (2.41), and (2.42). The above calculational scheme is then repeated for the additional time intervals. This scheme is numerically stable since iterative calculations are not required and, even with a reasonably high number of wing panels and wake elements, the vortex core distance from collocation points is far from being critical.

CHAPTER 3. RESULTS OF APPLICATIONS

3.1 Definition of the configurations

The program can handle any configuaritons of a wing. The number of inputs depends on the number of components of the configuration and on the detail used to describe each component. Three sets of inputs can be distinguished:

    (a) Configuration geometry input information, which defines the geometry

    (b) Parameters concerning the solution procedure, output desired and computation of aerodynamic influence coefficients

    (c) Free stream data. This defines the Mach number, angle of attack and angle of yaw

In the following each set of input cards is described in detail.

    (a) <u>First input card</u>

TITLE - It may contain any desired information identifying the configuration to be input.

REFWA - Reference area to be used to non-dimensionalize computed forces and moments on components of the configuration. If not specified its value is set equal to the default value 1.0

REFWS - Wing semi-span. If not specified a value of 1.0 is used as default value

REFWC - Wing reference chord, used to non-dimensionalize computed moments on components of the configuration. If not specified a default value of 1.0 is used

REFX - x-coordinate of the moment center. If not specified a default value of 0.0 is used

REFY - y-coordinate of the moment center. If not specified a default value of 0.0 is used

REFZ - z-coordinate of the moment center. If not specified a default value of 0.0 is used

NWS - Number of airfoil sections used to define the wing segment

KWX - Number of ordinates used to define each airfoil section of the segment

XWREF - This wing data records contain the KWX locations, in per cent chord from the airfoil leading edge, at which the coordinates of the NWS airfoils describing the segment are to be specified. The locations are given in increasing per cent chord order. Note that the ordinates of all NWS airfoils describing the segment are to be specified at the same set of per cent chord locations.

WFORG - The next NWS data records each contain 5 numbers, which define the origin x, y, and z values, chord length and the leading edge radius of the airfoil sections describing the wing segment. For each wing segment the airfoil section at the smallest y_{ref}-value is input first, followed by the airfoil section at second smallest y_{ref}-value, etc.

ZWREF - This set of records specifies the KWX values of the half-thickness at the corresponding KWX per-cent-chord locations of the NWS airfoil sections defining the segment and ordered in the same way. The half-thickness is expressed in per cent airfoil chord, and is defined here as being perpendicular to the plane parallel to the x_{ref}-axis and passing through the leading edge of the segment.

KWY - Number of airfoil sections used to panel the wing segment. If KWY = 0 the panel's streamwise edges are defined by the NWS airfoil sections, otherwise the program interpolated linearly between the airfoil section defined in (a) to obtain x_{ref} and z_{ref}-coordinates at the y_{ref}-coordinates to be specified below.

YWREF - This record contains KWY values of the y_{ref}-coordinate of the airfoil sections used to define the side edges of the panels. These values are arranged in the order starting at the airfoil at the lowest y_{ref} continuing with the airfoil at the second lowest y_{ref}, etc.

(b) Second input card

ITER - Wake iteration number. Iteration number is non-zero for unsteady wing solutions

LTS - 0   Permits both leading- and trailing-edge separation

       1   Permits only trailing-edge separation

    - 1   Permits only leading-edge separation

(c) Third input card

MACH - The Mach number, subsonic or incompressible, at which the aerodynamic data are to be computed.

ALPHA - The angle of attack, expressed in degrees, at which the free stream is inclined to the $z_{ref} = 0$ plane

YAW - The angle of sideslip, expressed in degrees, at which the free stream is inclined to the $y_{ref} = 0$ plane. Sideslip is zero for this version.

The wing segments first must be divided into a number of strips spanwise parallel to x-axis. This is a restriction for wing components. The wing components are divided into KYW strips times KXW streamwise panels on each strip.

In steady state solutions, the "lift-carry-over" segments must be handled separately, Fig. 12. It is noted before that the "lift-carry-over" segments do not have collocation points on them and have the singularity distributions equal to the first adjacent strip of the wing components. The wing components have panel type (A) on the wing and panel type (B) on the wake shown in Fig. 13.

In unsteady state solutions, wake segments have own collocation points like wing segments but they do not have source distributions. Also their panel type is similiar to wing components, panel type (A).

The configuration is geometrically and aerodinamically symmetric according to the $y_{ref}=0$ plane. This symmetry reduces the number of unknowns by half because applying the boundary conditions on the collocation points of the starboard side of the configuration will be enough. The influence of the port side of the configuration to the starboard side should be included in the influence coefficients matrix. The singularity strengths will be identical for the symmetry panels. Also in steady case, the flow around the configuration may be computed for different angles of attack without solving the system of equations again.

3.2 Structure of the computer code "WAERO"

In this section, a short description is given of the capabilities of the computer code developed. This code consists of seven main subroutines in the three part as follows;

(a) <u>Geometry</u>

WINPAN - This subroutine reads necessary data from input files. The geometry of each segment is defined by its planform and any number (>1) of airfoil sections. The airfoil sections are described at the same array of percentage-chord positions. From the input data on the geometry and additional data on the desired panel scheme for the configuration the program computes coordinates of panel corner points and panel collocation points, panel inclination and incidence, panel area, etc. All these data, which are needed in the computation of the aerodynamic influence coefficients, are stored on auxilliary files.

(b) <u>Aerodynamics and Solutions</u>

INFWIN - This subroutine calculates aerodynamic influence coefficients matrix for wing panels $[A_b]$ which are effected by the other wing panels. The geometric knowledge which are in the auxilliary files are used in this calculation procedure. For the unsteady case after the first time step, for wing panels $[A_l]$ and $[A_t]$ matrices which are effected by leading- and trailing-edge wake panels are computed in this subroutine.

SOLWIN - This subroutine solves the aerodynamic influence coefficients matrices based on wing panels according to the Gauss elimination method by partial pivoting of coefficients.

INFWAK - This subroutine calculates aerodynamic influence coefficients matrix for wake panels $[A_{bw}]$ which are effected by the wing panels. Also, $[A_{lw}]$ and $[A_{tw}]$ matrices which are effected by the other wake panels are computed in this subroutine.

SOLWAK - This subroutine solves the aerodynamic influence coefficients matrices based on wake panels according to the Gauss elimination method by partial pivoting of coefficients.

MOVE - This subroutine translates the wake elements with downwash velocity components to the new locations.

(c) Results

WCALC - In steady case, the pressure distribution on the wing is computed using the first-order formula of the Bernoulli equation. In the same fashion in unsteady case, nonsteady term is added to the Bernoulli equation for pressure calculations. The output of this subroutine consists of pressure distribution, forces and moments.

MCALC - This subroutine is computed velocity distribution on the wing for given time step and found the Mach distribution around the wing.

3.3 Results

The computational method dealt with two different kinds of wing geometry. First geometry is rectangular planform wing geometry. Aspect ratio is 2.0, profile of the wing is supersonic, symmetric profile which described in Fig. 14. All wing geometries divided to 200 panels and all analysis are in subsonic region with small angle of attack.

The output data of the present code are shown on the 3-D images of the geometries as pressure coefficients (C_p) and mach contour distributions which includes both upper and lower surface of the wing geometry. The results of the rectangular wing geometry with respect to angle of attack at two different Mach numbers are shown in Fig. 15 to 20, respectively. Fig. 21 illustrates 3-D images of the pressure coefficients and topological behaviour of the pressure contours at zero degree angle of attack. In this figure, Elliptic pressure distribution over the wing is easily seen. Figures 22, 23 also illustrate same thing at ten degrees angle of attack. Fig. 24 shows pressure differences between upper and lower surface of the wing at ten degrees angle of attack.

Second geometry is 70 degrees swept angle delta wing. Figure 25 gives some information about this wing geometry, profile of the wing is same with first geometry. Figure 26 to 31 illustrate the results of pressure coefficients around the delta wing. Figure 32 shows the pressure distribution evaluation with the angle of attack at some different location on the wing.

It can easily seen that pressure will grew up with the angle of attack, directly.

Figure 33 and 34 shows that classical wake development differences from unsteady wake development. Both of this figures are in 0.6 Mach number, 0 degree angle of attack. In unsteady wake development $\Delta t = 0.1$ and time is $t = 0.2$. Fig. 35 includes lift, drag and rolling moment coefficients behaviour with angle of attack at classical wake solutions.

CHAPTER 4. CONCLUSIONS

The present thesis is based on the potential theory. The aim of the thesis was to comparison the unsteady wake development with classical wake approximation "panel" methods at incompressible and subsonic flows around different wing geometries. The results and outputs of applications show that, the subsonic flow is well modeled with classical wake approximation. In the unsteady case, the non-iterative technique was developed and this technique must be improved and used in a lot of configuration and flow regimes.

Also there exist possibilities for improving the computational efficiency of both methods through:

- vectorization and/or parallelization on supercomputers
.- reduction of operational count for the evaluation of influence integrals
- new formulations and improve numeric techniques.

FIGURES
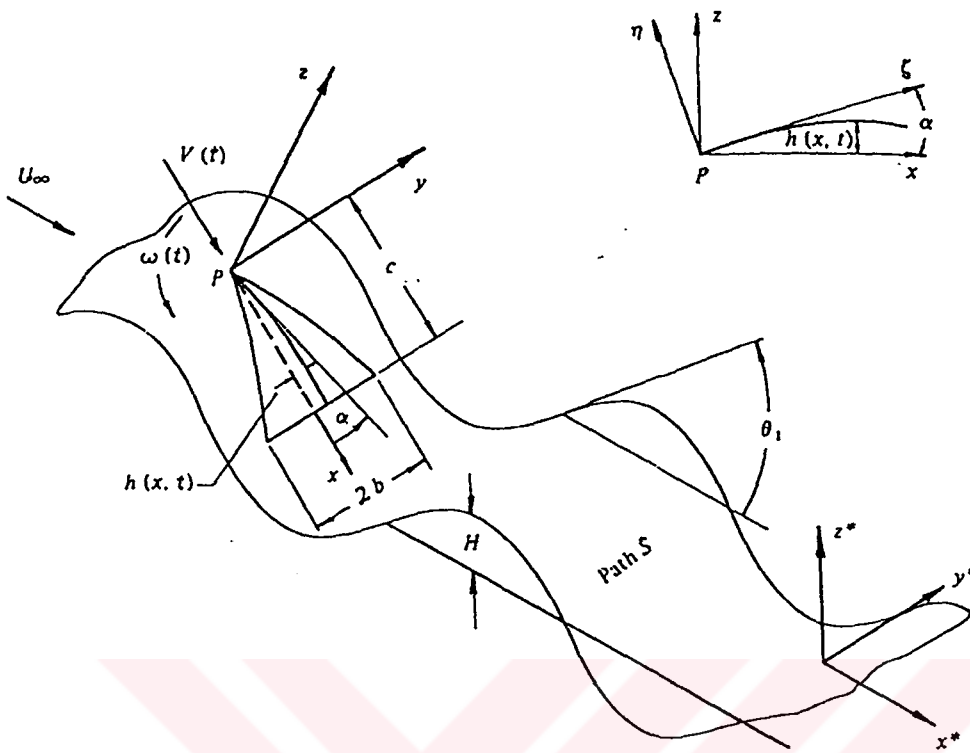
Figure 1.   Schematic description of the foil motion and the co-ordinate systems used.
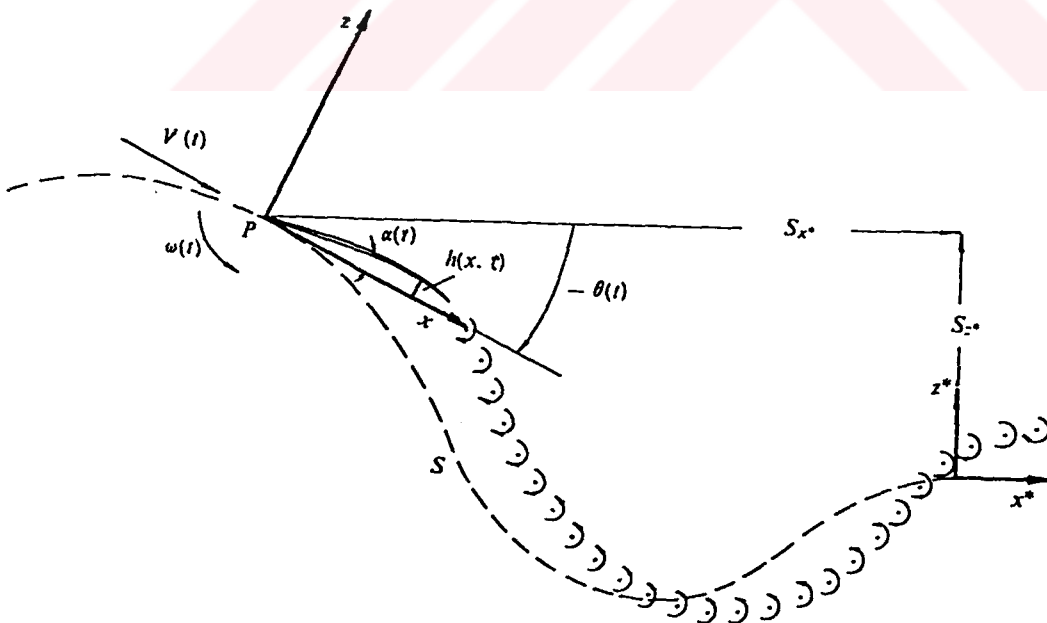
Figure 2.   Schematic description of the wake model.

THE UNIVERSAL SOURCE

- **SUPERIMPOSE CONTINUOUS SERIES OF PULSES**

$$\phi_s = \int_0^t \frac{\sigma(t^*)}{4\pi} \frac{\delta(t-t^*-\rho/a)}{\rho} \, dt^*$$

$$\phi_s = \sum_{i=1}^m \frac{\sigma(t-\tau_i)}{4\pi R_i}$$

$$R_i = \rho_i |\vec{V}_T \cdot \vec{n}|_i \, /a$$

$$\tau_i = t - t_i^*$$
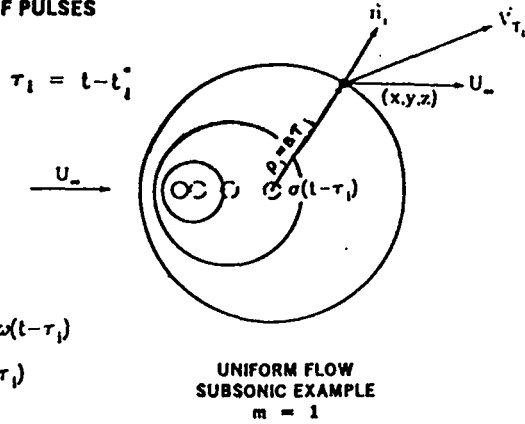
- **STEADY FLOW —** $\sigma(t-\tau_i) = \sigma_0$
- **OSCILLATORY FLOW —** $\sigma(t-\tau_i) = \sigma_0 e^{i\omega(t-\tau_i)}$
- **TRANSIENT FLOW —** $\sigma(t-\tau_i) = f(t-\tau_i)$
- **SUBSONIC FLOW —** $m = 1$
- **SUPERSONIC FLOW —** $m = 2$ OR $m = 0$
- **ACCELERATED OR DECELERATED FLOW —** $m = 1, 2, 3$ etc.
- **NONUNIFORM TRANSONIC FLOW —** $m = 1, 2, 3$ etc.

**UNIFORM FLOW
SUBSONIC EXAMPLE
m = 1**

UNIFORM FLOW

$$\phi_s = \frac{\sigma(t-\tau)}{4\pi R}$$

$$\tau = \frac{M}{U_\infty \beta^2}[R - M(x-\xi)]$$

$$R = \sqrt{(x-\xi)^2 + \beta^2 r^2} \quad \text{HYPERBOLIC RADIUS}$$

$$\beta^2 = 1 - M^2$$
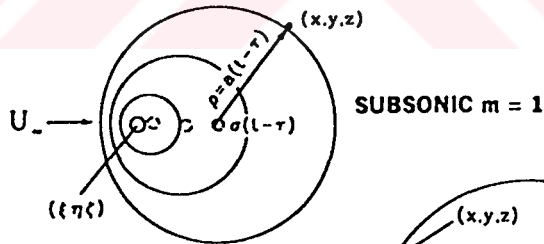
$$\phi_s = \frac{\sigma(t-\tau_1)}{4\pi R_1} + \frac{\sigma(t-\tau_2)}{4\pi R_2}$$

$$R_1 = R_2 = R$$

$$\tau_1 = \frac{M}{U_\infty \beta^2}[R - M(x-\xi)]$$

$$\tau_2 = \frac{-M}{U_\infty \beta^2}[R + M(x-\xi)]$$

$$\beta^2 = 1 - M^2$$

SUBSONIC m = 1

**SUPERSONIC m = 2
OR m = 0**
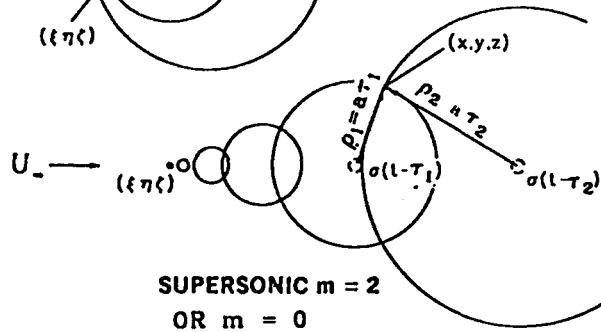
Figure 3.   Schematic description of the universal source and uniform flow, in Reference [11].

POTENTIAL DOUBLET
(DOUBLE SOURCE)

DOUBLE SOURCE   DOUBLET

$$\frac{\partial \phi_s}{\partial N} = \frac{\partial}{\partial N}\left(\frac{\Delta\phi(\iota-T)}{4\pi R}\right) = \phi$$
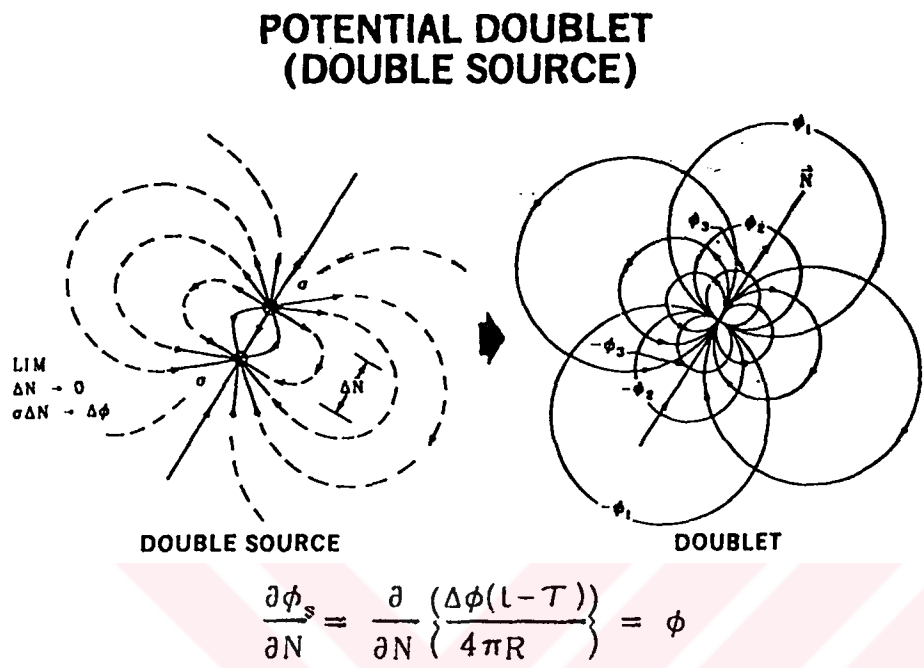
Figure 4.   Schematic description of the potential doublet, Ref. [11].

RELATION OF DOUBLET DISTRIBUTIONS
TO VORTEX LINES

DOUBLET SHEETS   VORTEX LINES
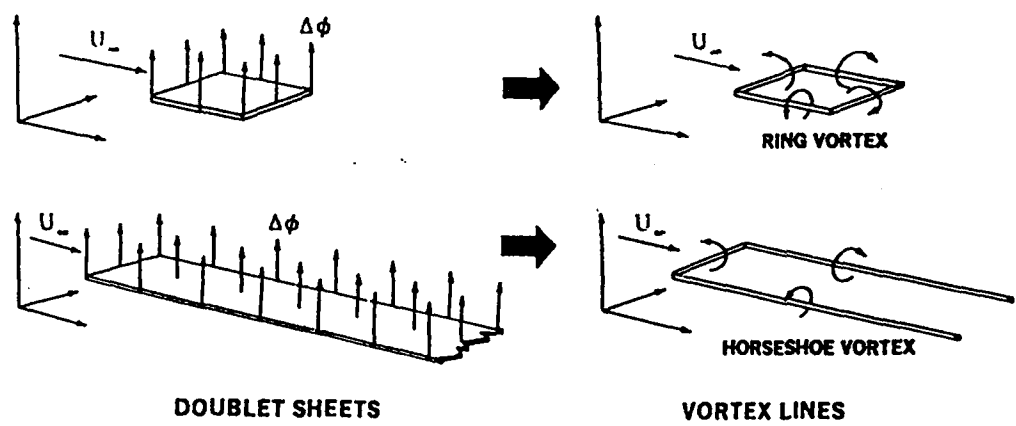
Figure 5.   Relation of doublet distributions to vortex lines, Ref. [11].

PRESSURE DOUBLET

- IF φ SATISFIES BASIC DIFFERENTIAL EQUATION THEN SO DO φ_x, φ_t AND ANY LINEAR COMBINATION VIZ C_P

$$\varphi_x = \frac{\partial}{\partial N}\left\{\frac{\Delta\varphi_x(t-\tau)}{4\pi R}\right\}$$

$$\varphi_t = \frac{\partial}{\partial N}\left\{\frac{\Delta\varphi_t(t-\tau)}{4\pi R}\right\}$$

$$C_P = -\frac{2}{U_\infty}\left\{\varphi_x + \varphi_t/U_\infty\right\}$$

$$C_P = \frac{\partial}{\partial N}\left\{\frac{\Delta C_P(t-\tau)}{4\pi R}\right\}$$

$-\Delta\varphi(x,t)$ $(\Delta\varphi_x = -\Delta\varphi_t/U_\infty)$

$\Delta C_P = 0$

PRESSURE DOUBLET PRESSURE FIELD

EQUIVALENT VELOCITY DOUBLET DISTRIBUTION
EACH PRESSURE DOUBLET HAS ITS OWN WAKE AND SATISFIES THE LINEARIZED KUTTA CONDITION
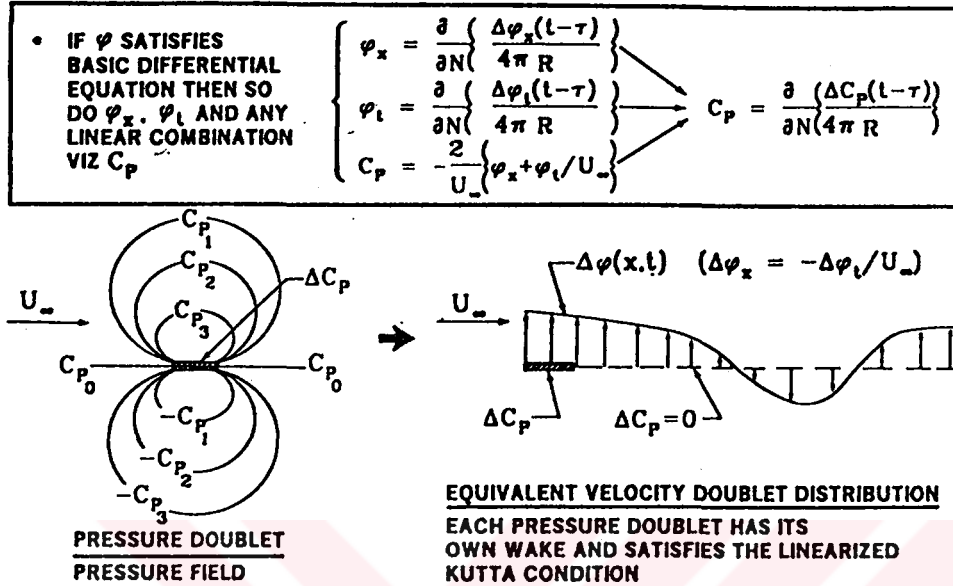
PRESSURE DOUBLET IN UNIFORM SUBSONIC SIMPLE HARMONIC MOTION

$$\Delta C_P(t-\tau) = \Delta C_P \exp[i\omega(t-\tau)] \quad \text{SIMPLE HARMONIC MOTION}$$

$$\tau = \frac{M}{U_\infty\beta^2}[R - M(x-\xi)] \quad \text{UNIFORM SUBSONIC FLOW}$$

$$C_P = \frac{\Delta C_P}{4\pi}\frac{\partial}{\partial N}\left\{\frac{\exp\{i\omega[t-\frac{M}{U_\infty\beta_s}(R-M(x-\xi))]\}}{R}\right\}$$

$$+$$

$$C_P = -2/U_\infty(\varphi_x + i\omega\varphi/U_\infty)$$

$$\varphi = -\frac{\Delta C_P}{8\pi}\int_{\xi}^{\infty}\frac{\partial}{\partial N}\left\{\frac{\exp(t-\tau(\bar\xi))}{R}\right\}\left[\exp[i\omega(\bar\xi-\xi)/U_\infty]\right]d\bar\xi$$

z,ζ

$$-\Delta\varphi = \Delta C_{P_0}\left[\exp[-i\omega(\bar\xi-\xi)/U_\infty]\right]$$

WAKE $\Delta C_P = 0$

$x,\xi,\bar\xi$ ΔC_P
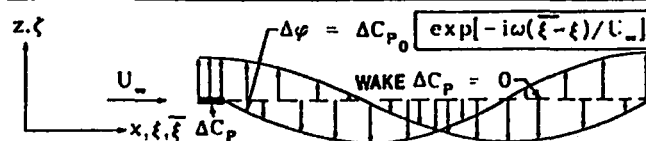
Figure 6. Schematic description of the pressure doublet, Ref. [11].
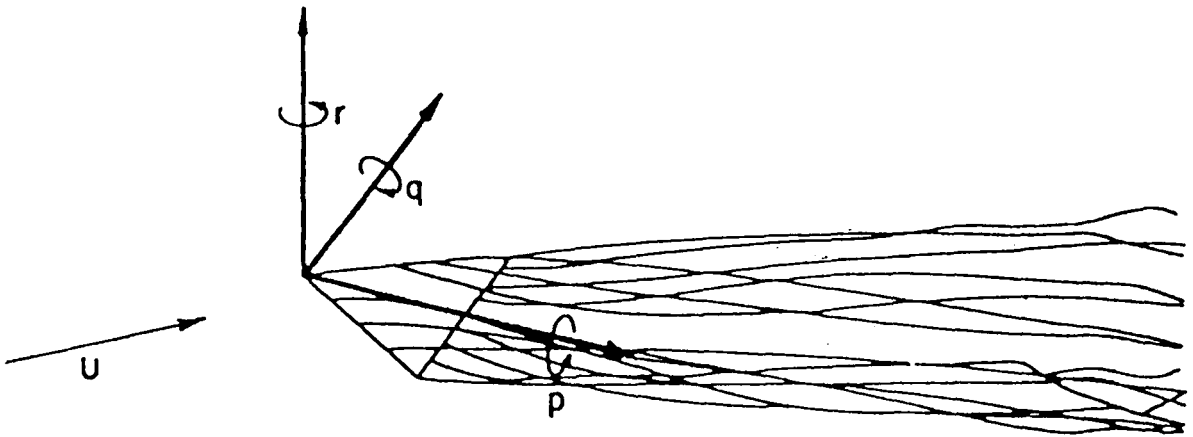
Figure 7.   Overview of the wing planform and co-ordinate system.
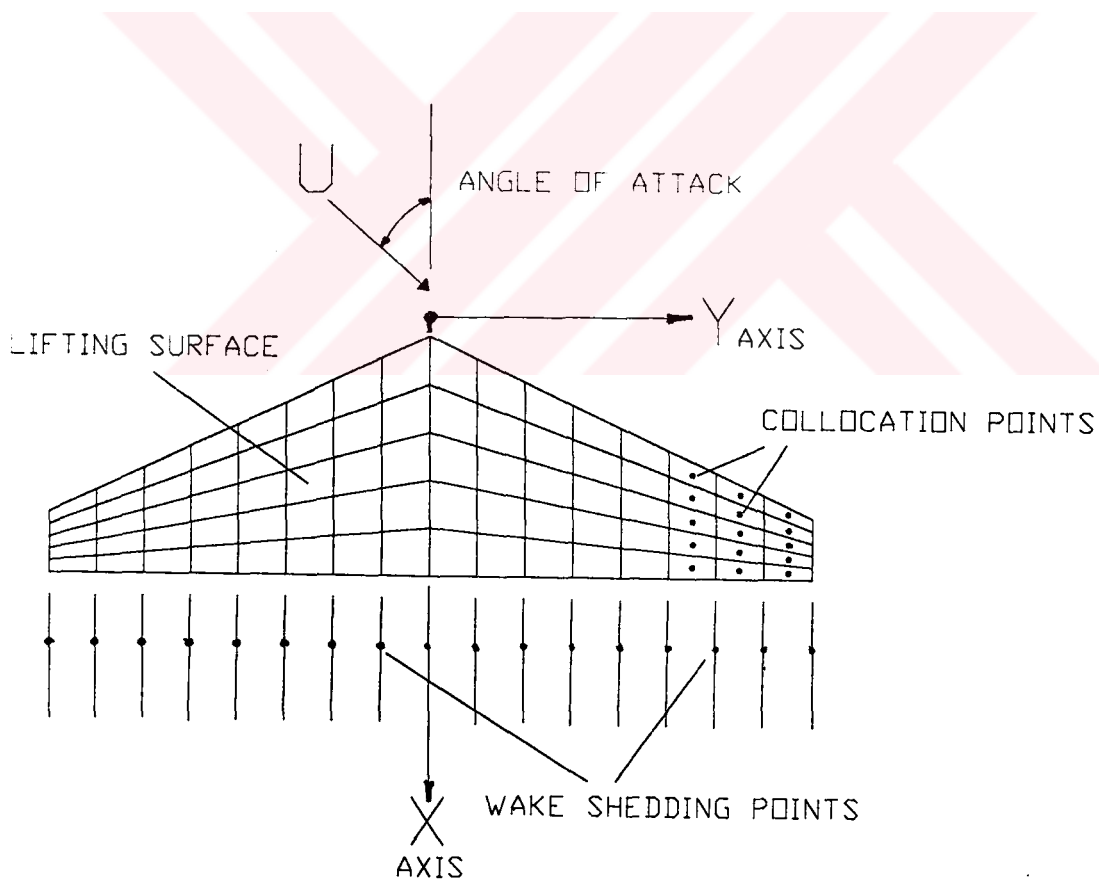
Figure 8.   The panel scheme on the configuration.
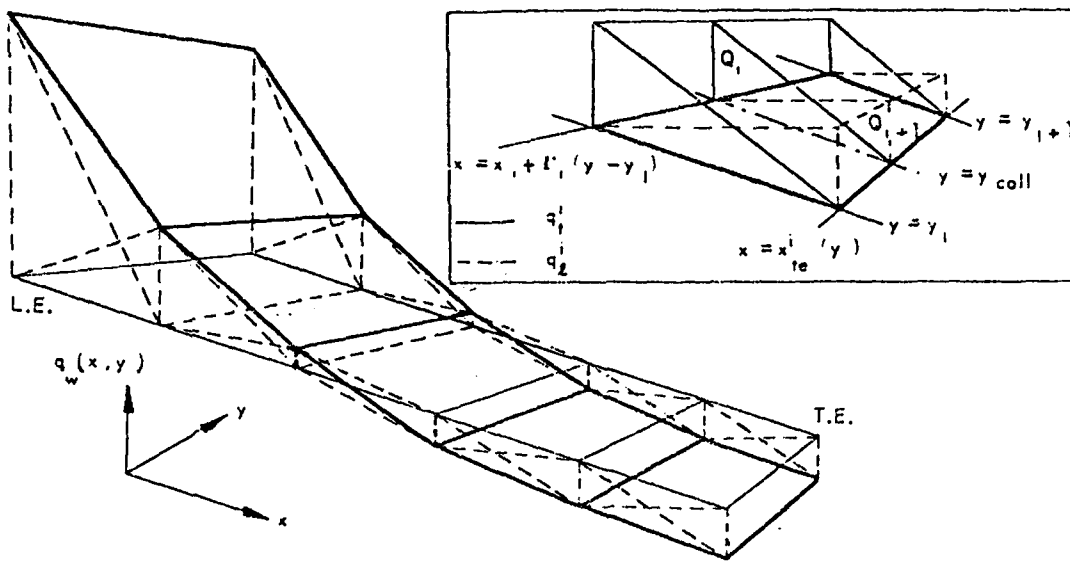
Figure 9.   The source distribution on a strip of the wing.
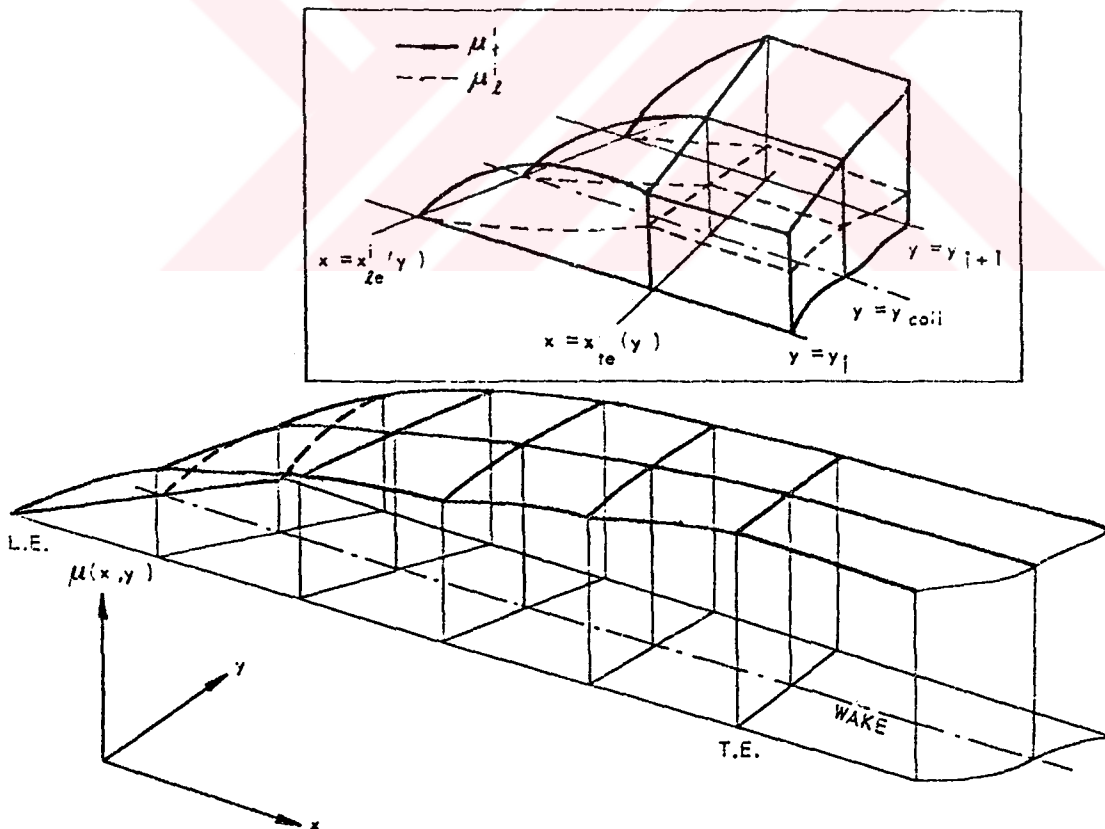
Figure 10.   The doublet distribution on a strip of the wing.
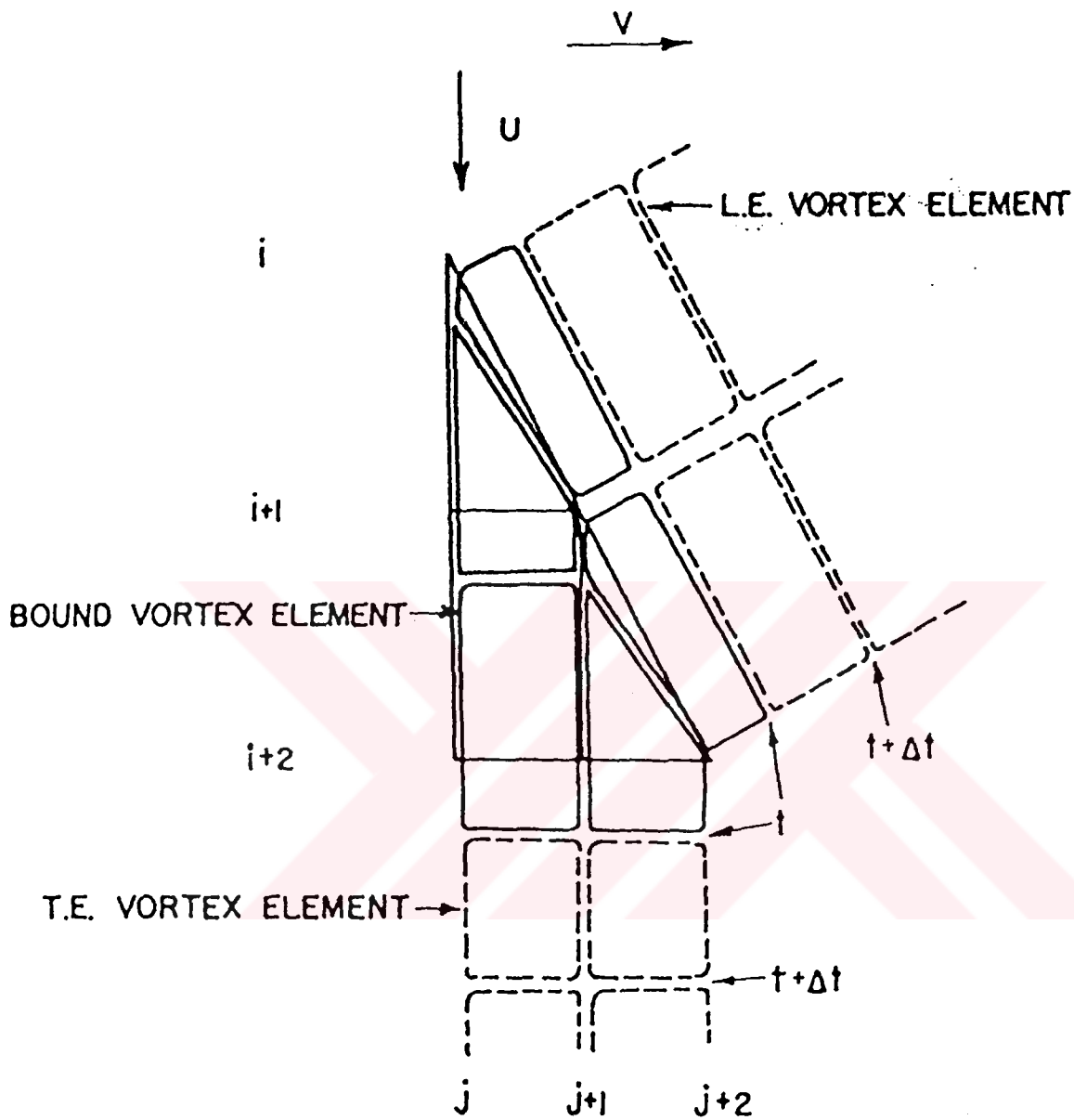
Figure 11. Release of the vortex segments at leading- and trailing-edge.
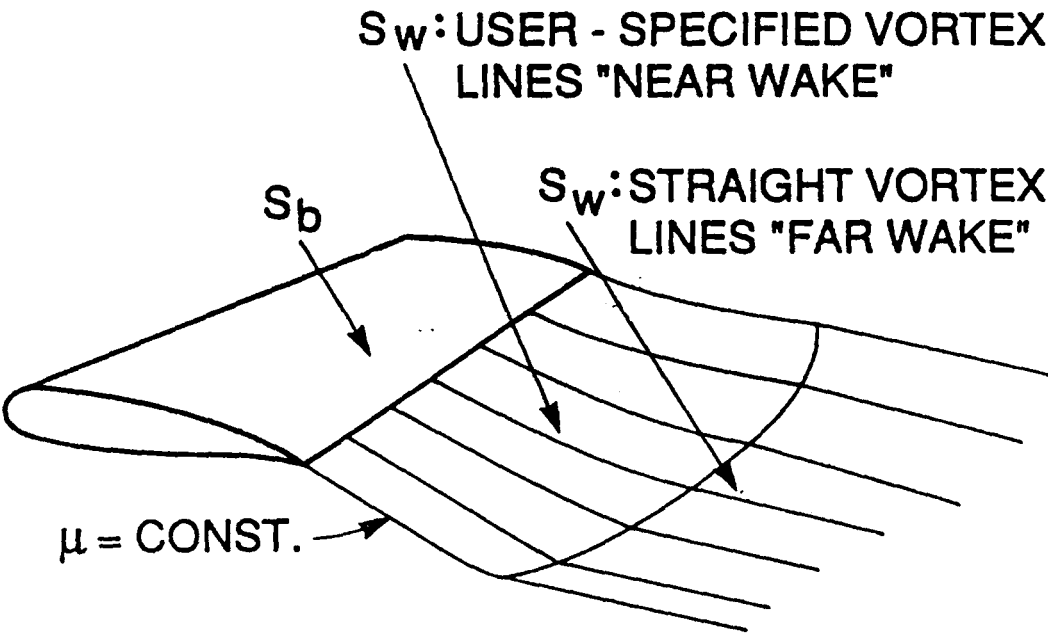
Figure 12. Wake surface at steady panel method algorithm.
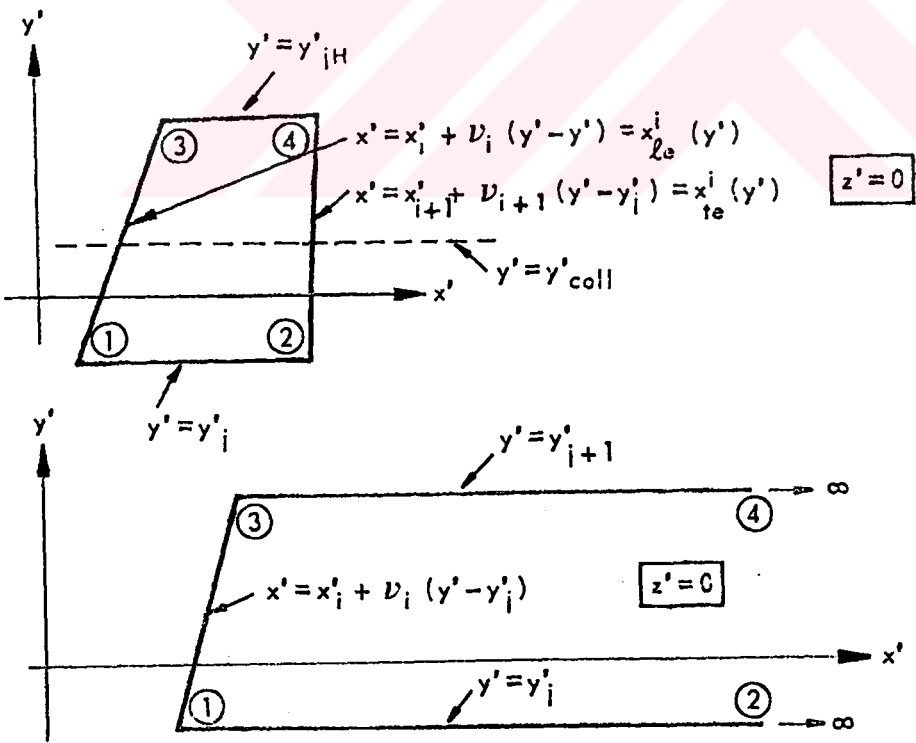
Figure 13. Panel types used at steady panel method algoritm.
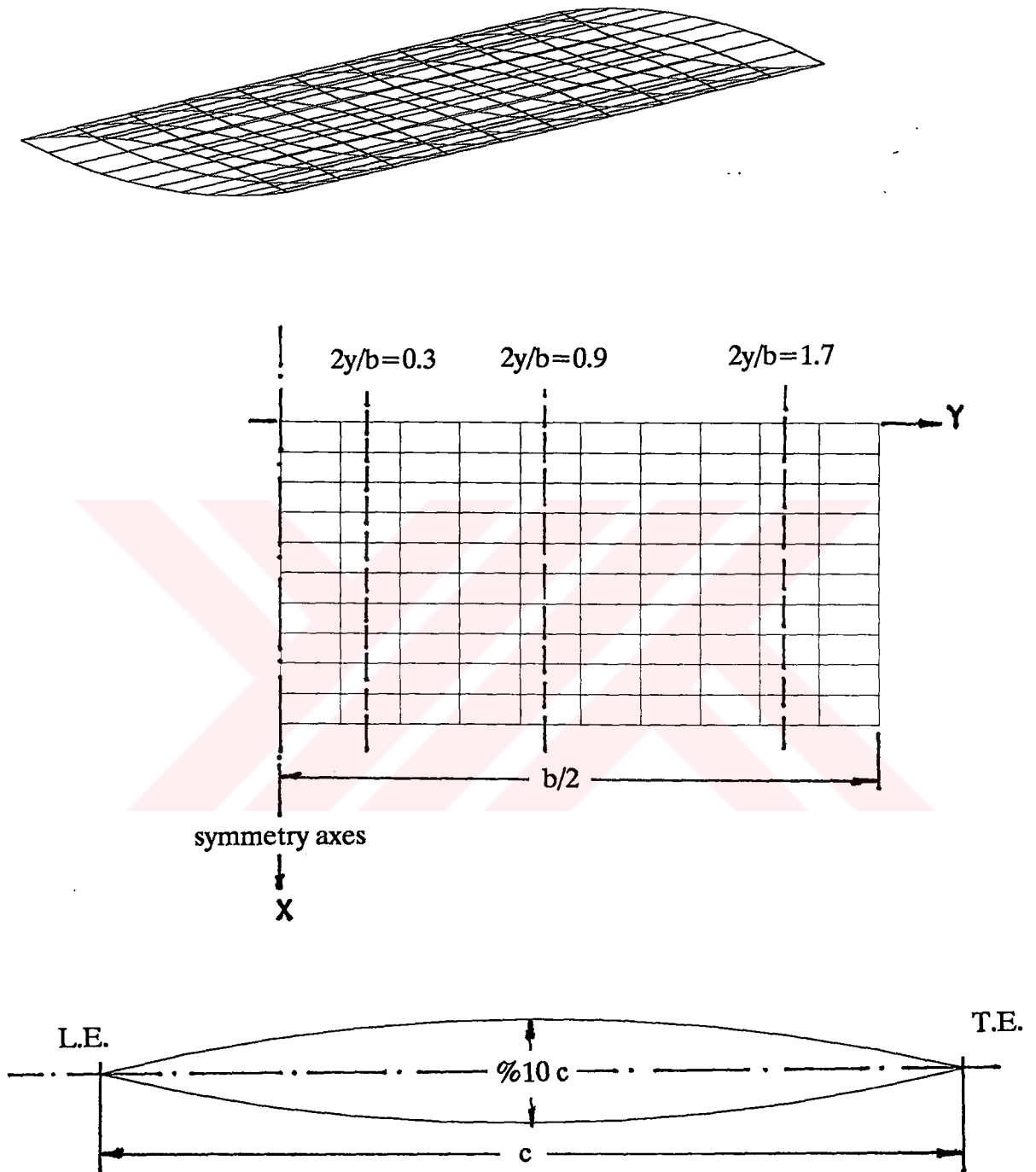
Figure 14.   Geometric definition of the rectangular wing.

M=0.4   M=0.6
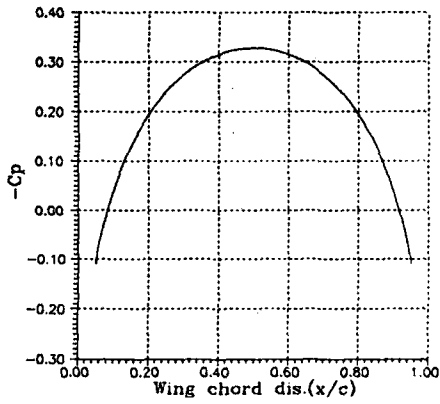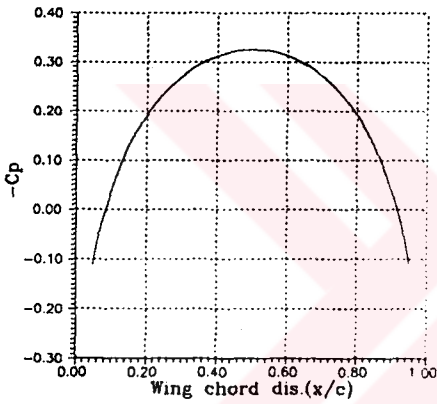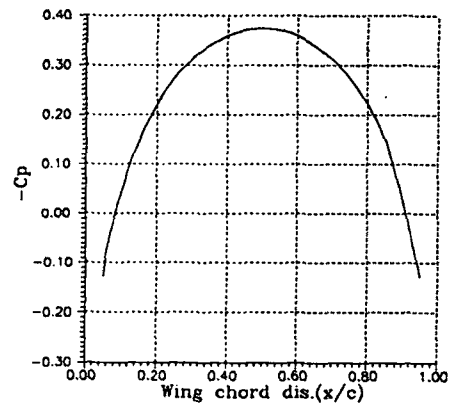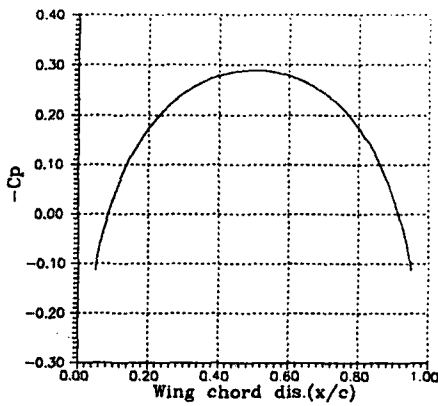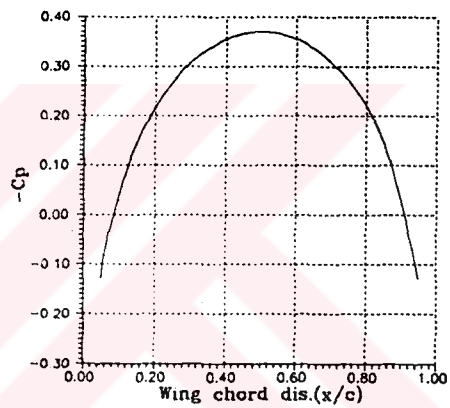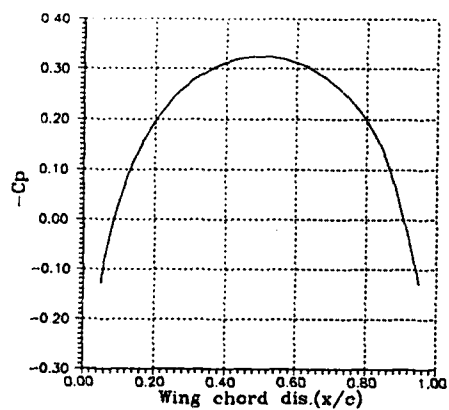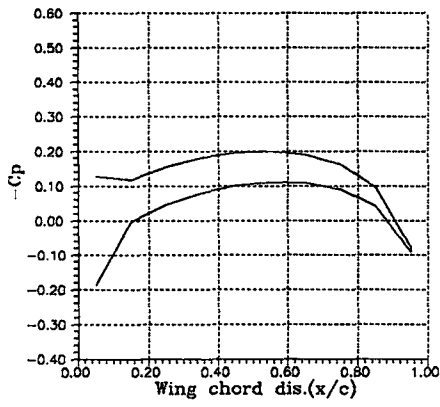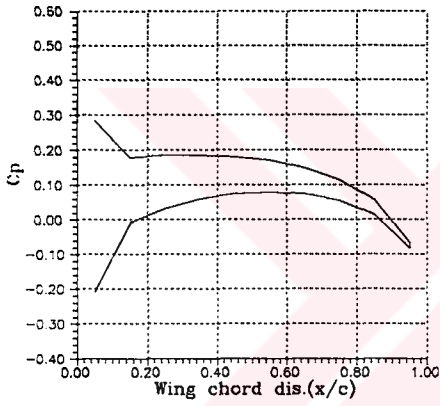

Figure 15.   Pressure distribution over the rectangular wing with 0° angle of
             attack at different locations
             (a) 2y/b = 0.3   (b) 2y/b = 0.9   (c) 2y/b = 1.7
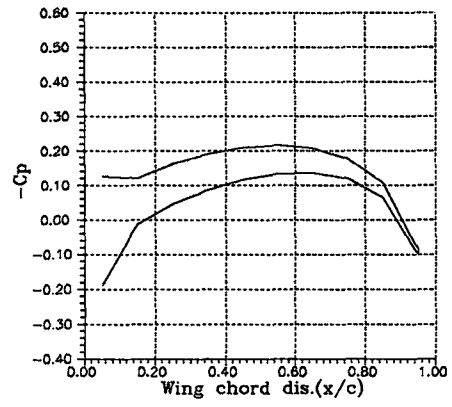
M=0.4

M=0.6

(a)

(b)

(c)
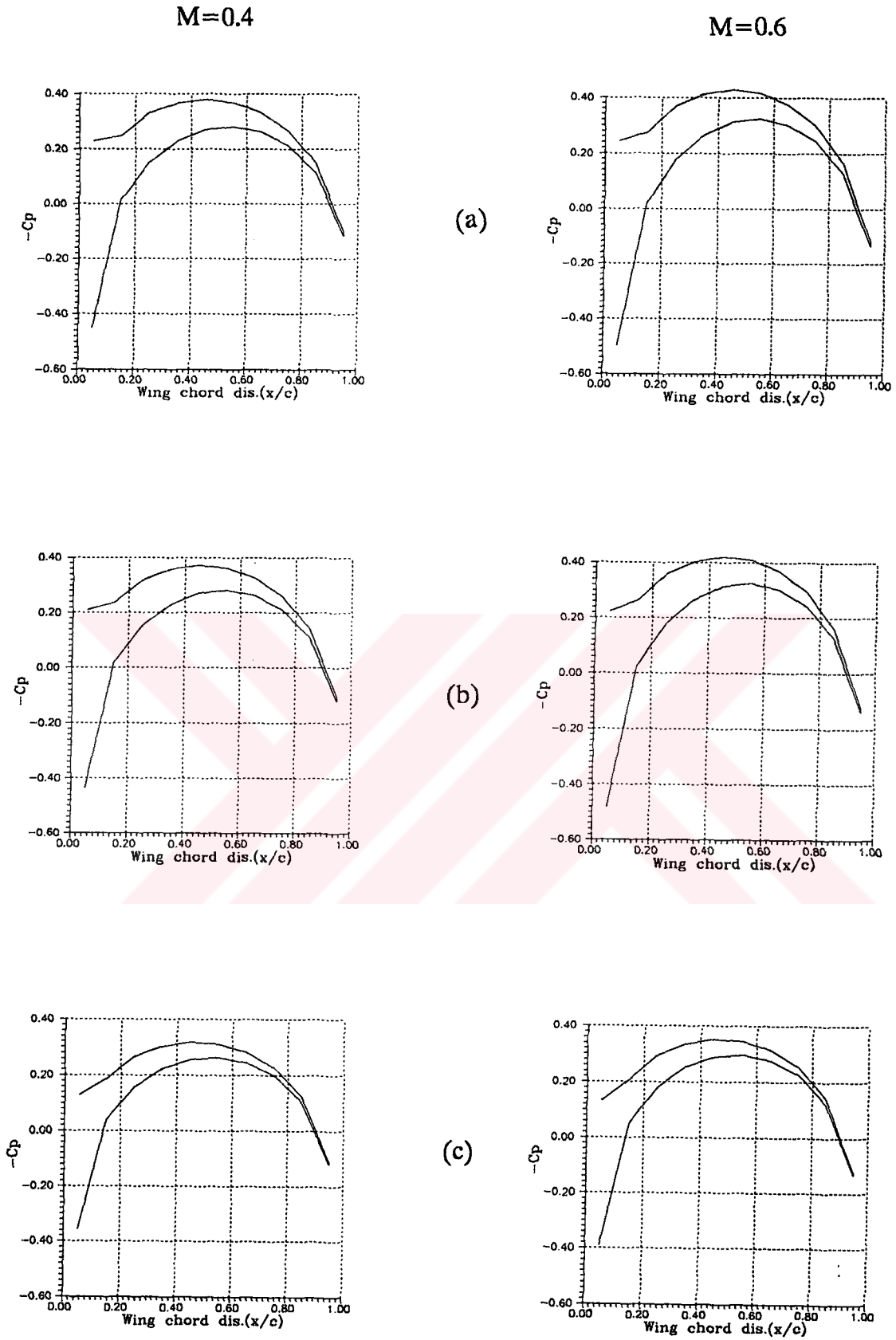
Figure 16. Pressure distribution over the rectangular wing with 2° angle of attack at different locations
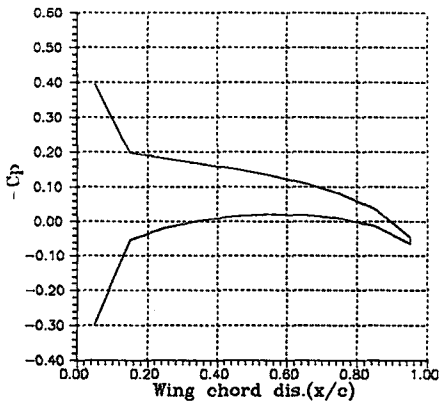
(a) 2y/b = 0.3   (b) 2y/b = 0.9   (c) 2y/b = 1.7

M=0.4

M=0.6

(a)

(b)

(c)
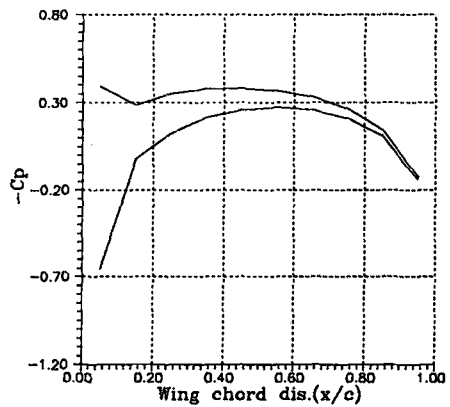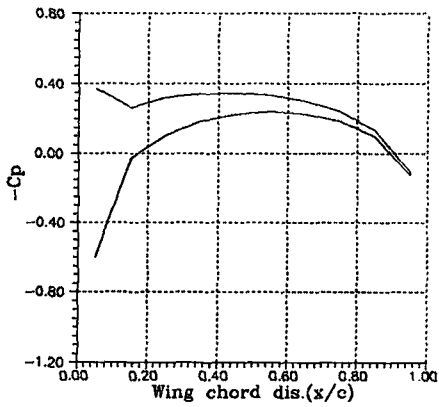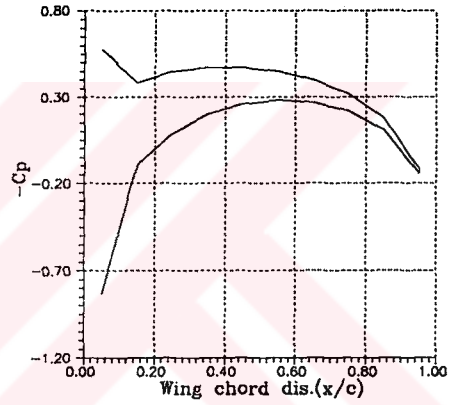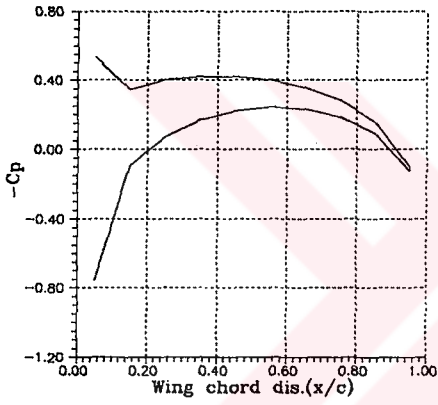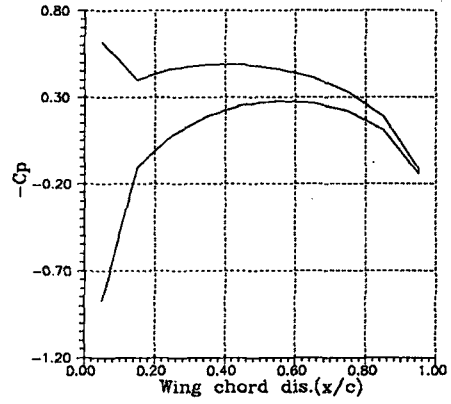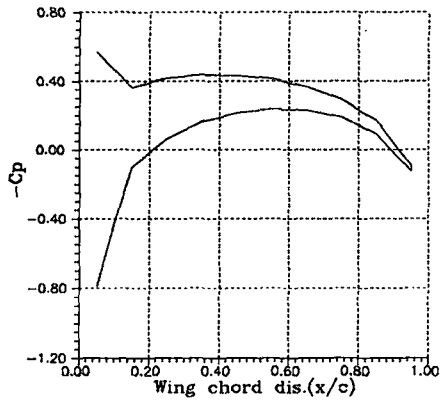
Figure 17. Pressure distribution over the rectangular wing with $4°$ angle of attack at different locations
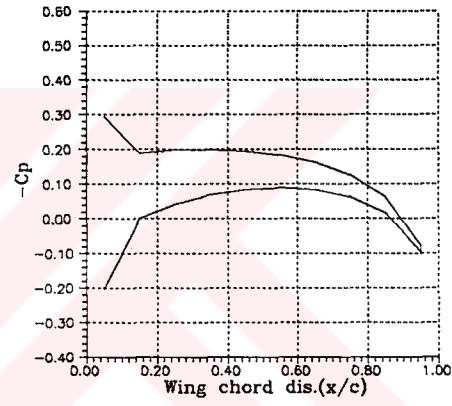
(a) $2y/b = 0.3$ (b) $2y/b = 0.9$ (c) $2y/b = 1.7$
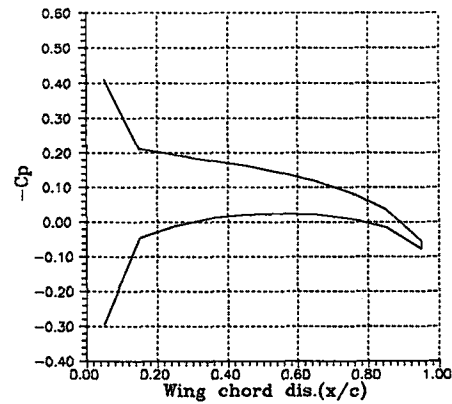
M=0.4

M=0.6

(a)

(b)

(c)
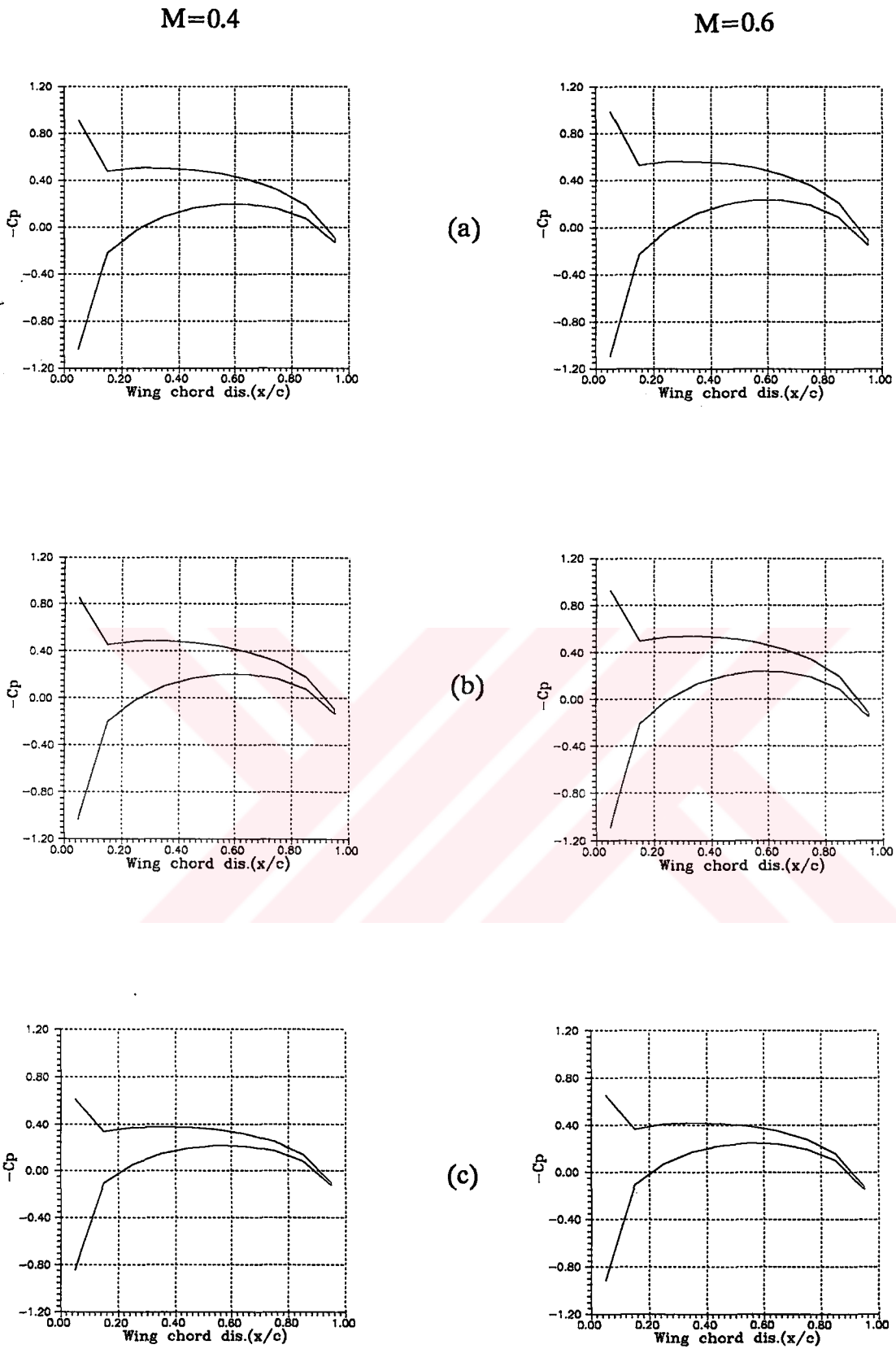
Figure 18. Pressure distribution over the rectangular wing with 6° angle of attack at different locations

(a) 2y/b = 0.3   (b) 2y/b = 0.9   (c) 2y/b = 1.7
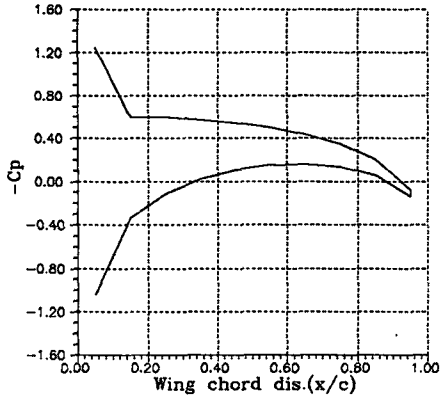
M=0.4   M=0.6
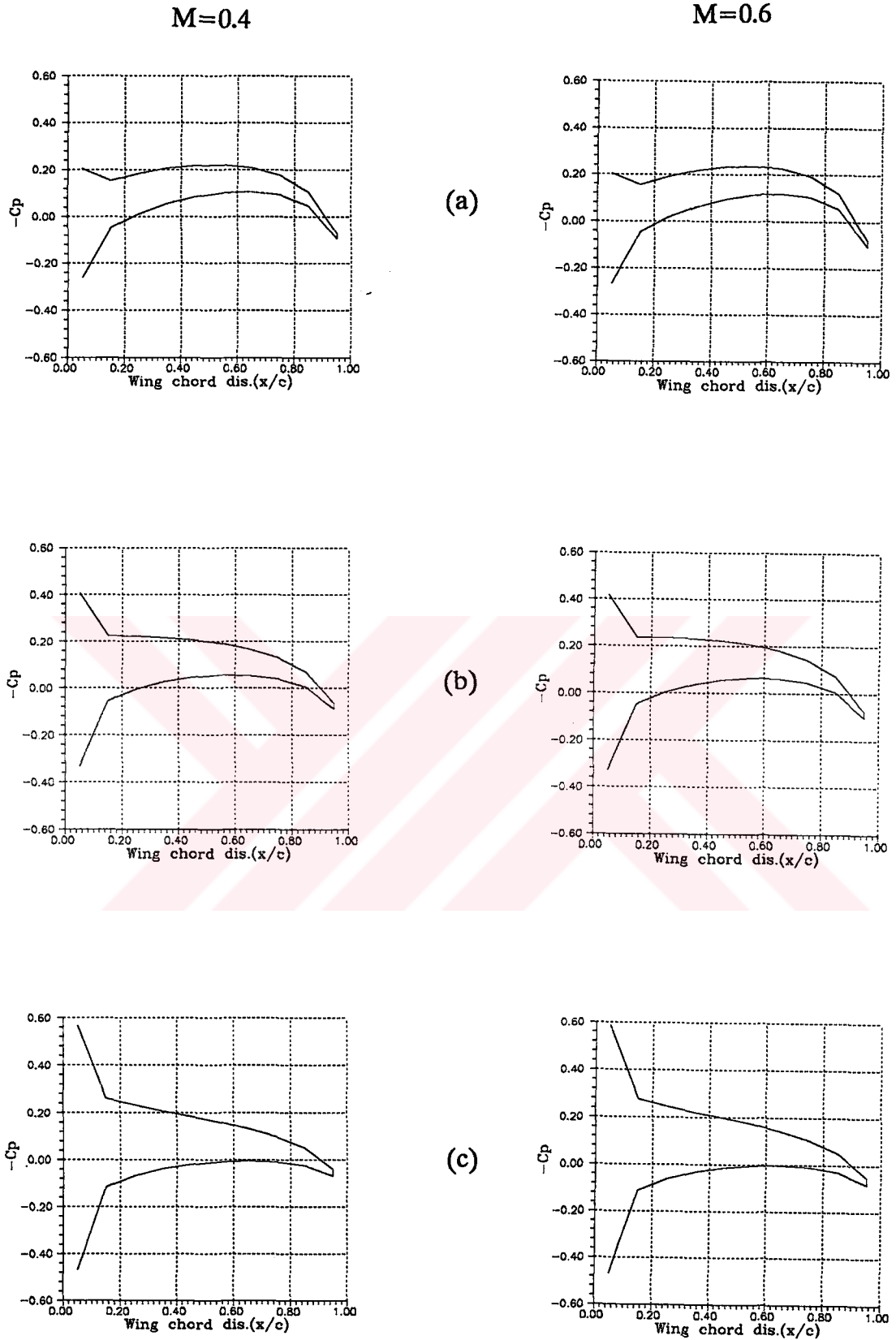

(a)
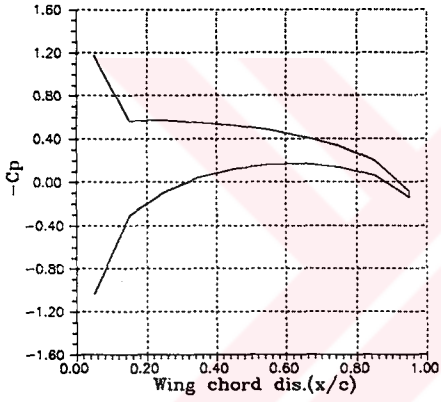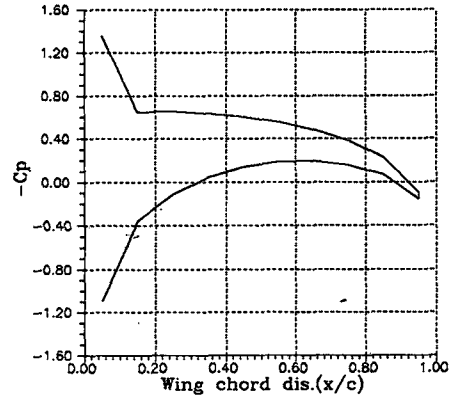
(b)
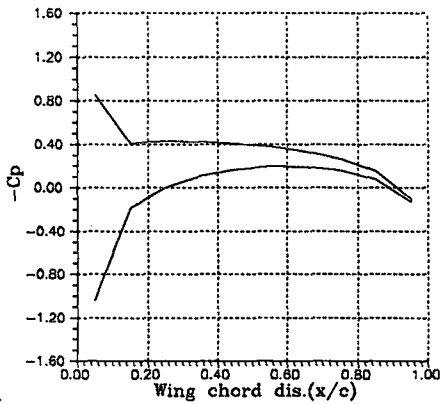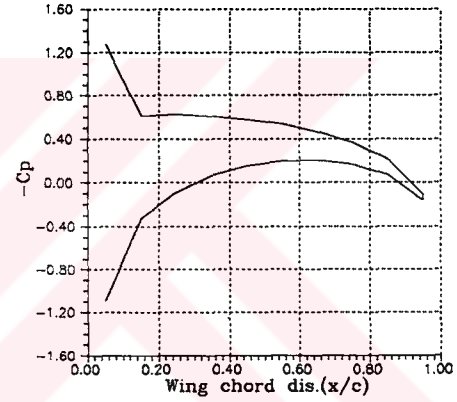
(c)
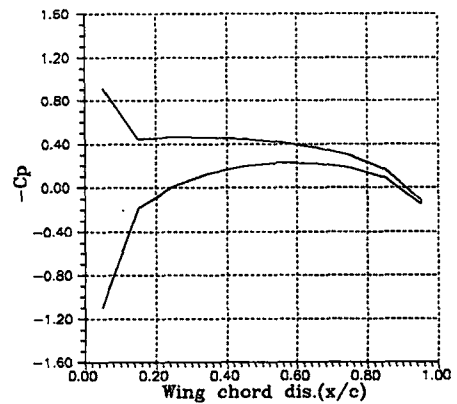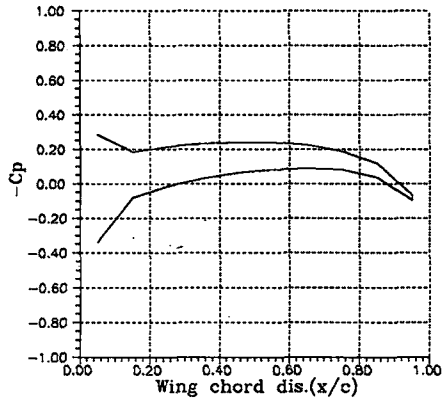
Figure 19. Pressure distribution over the rectangular wing with 8° angle of attack at different locations

(a) 2y/b = 0.3   (b) 2y/b = 0.9   (c) 2y/b = 1.7

M=0.4

M=0.6
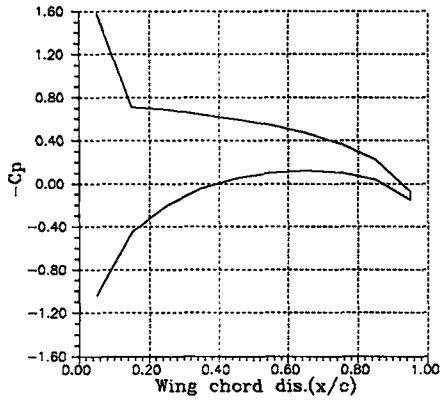
(a)
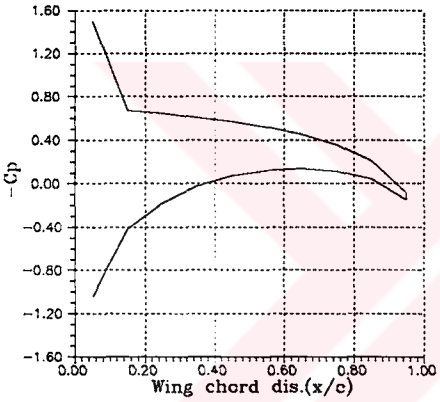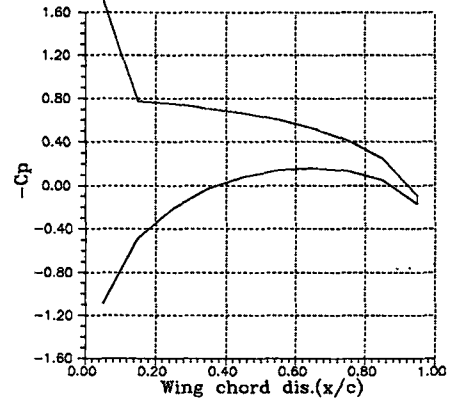
(b)
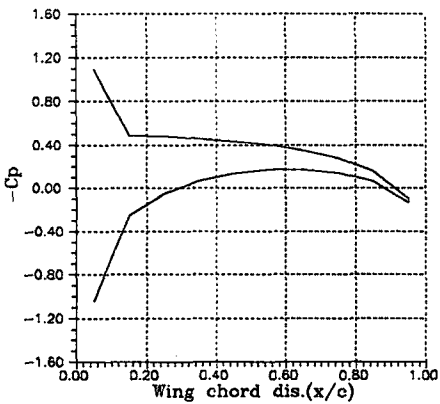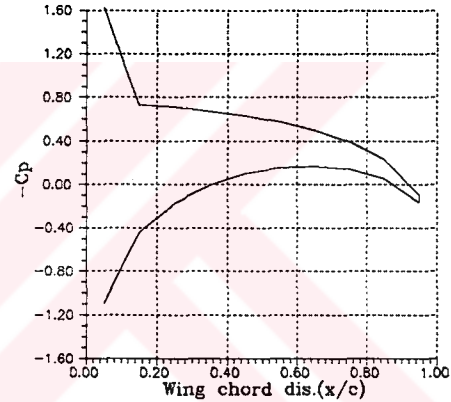
(c)
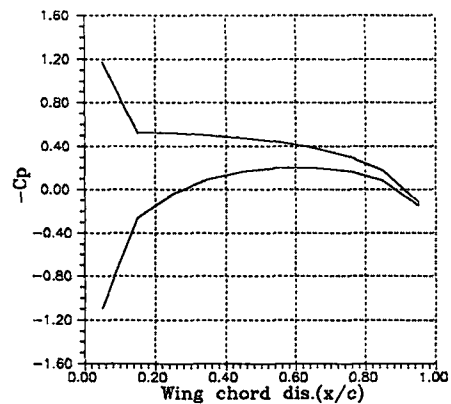
Figure 20. Pressure distribution over the rectangular wing with $10°$ angle of attack at different locations

(a) 2y/b = 0.3　　(b) 2y/b = 0.9　　(c) 2y/b = 1.7

PRESSURE CONTOURS ON RECTANGULAR WING
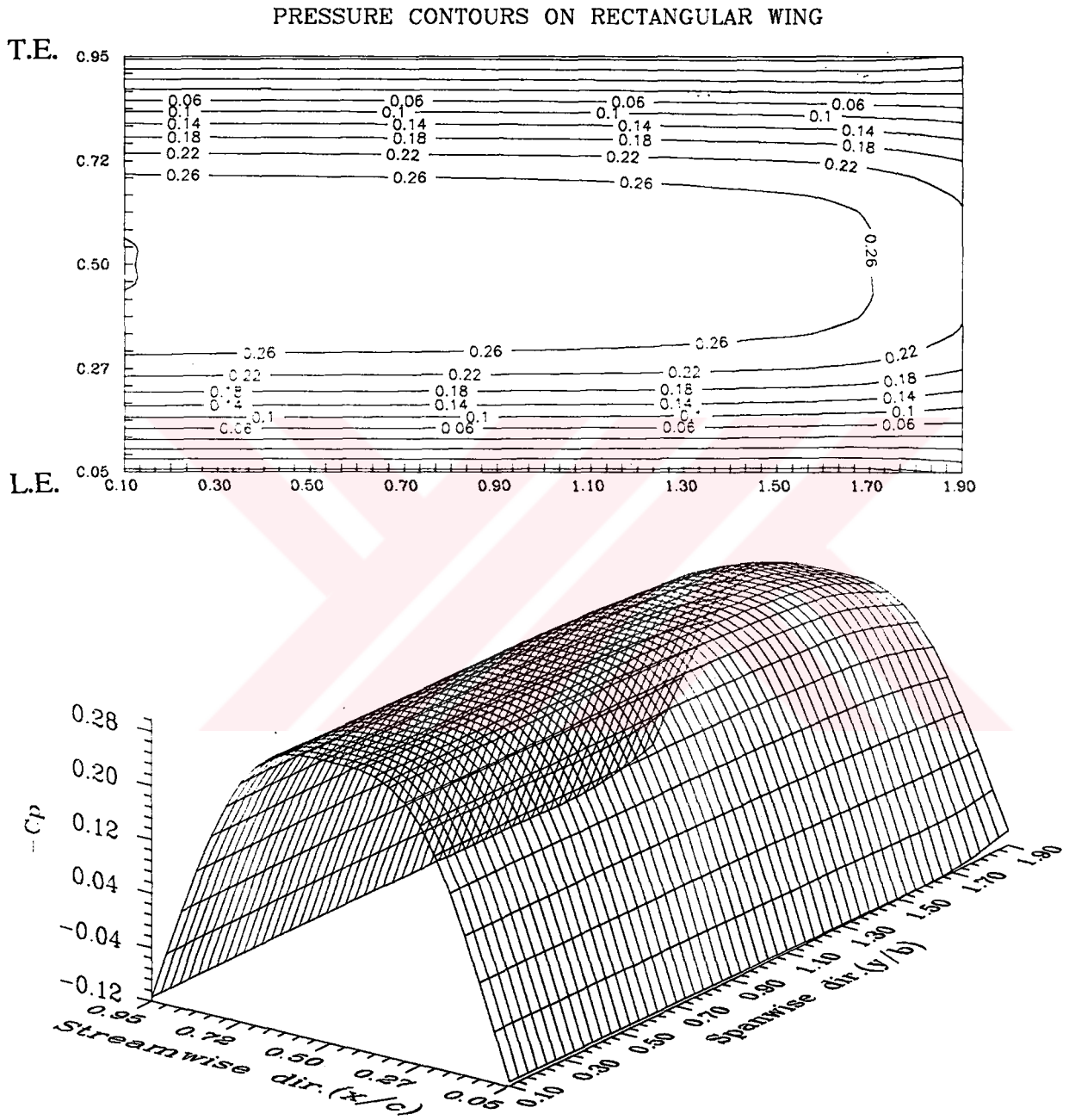
Figure 21.   3-D graphical representation and topology contours of the
pressure coefficient distribution over the wing at 0° angle of
attack

PRESSURE CONTOURS ON RECTANGULAR WING
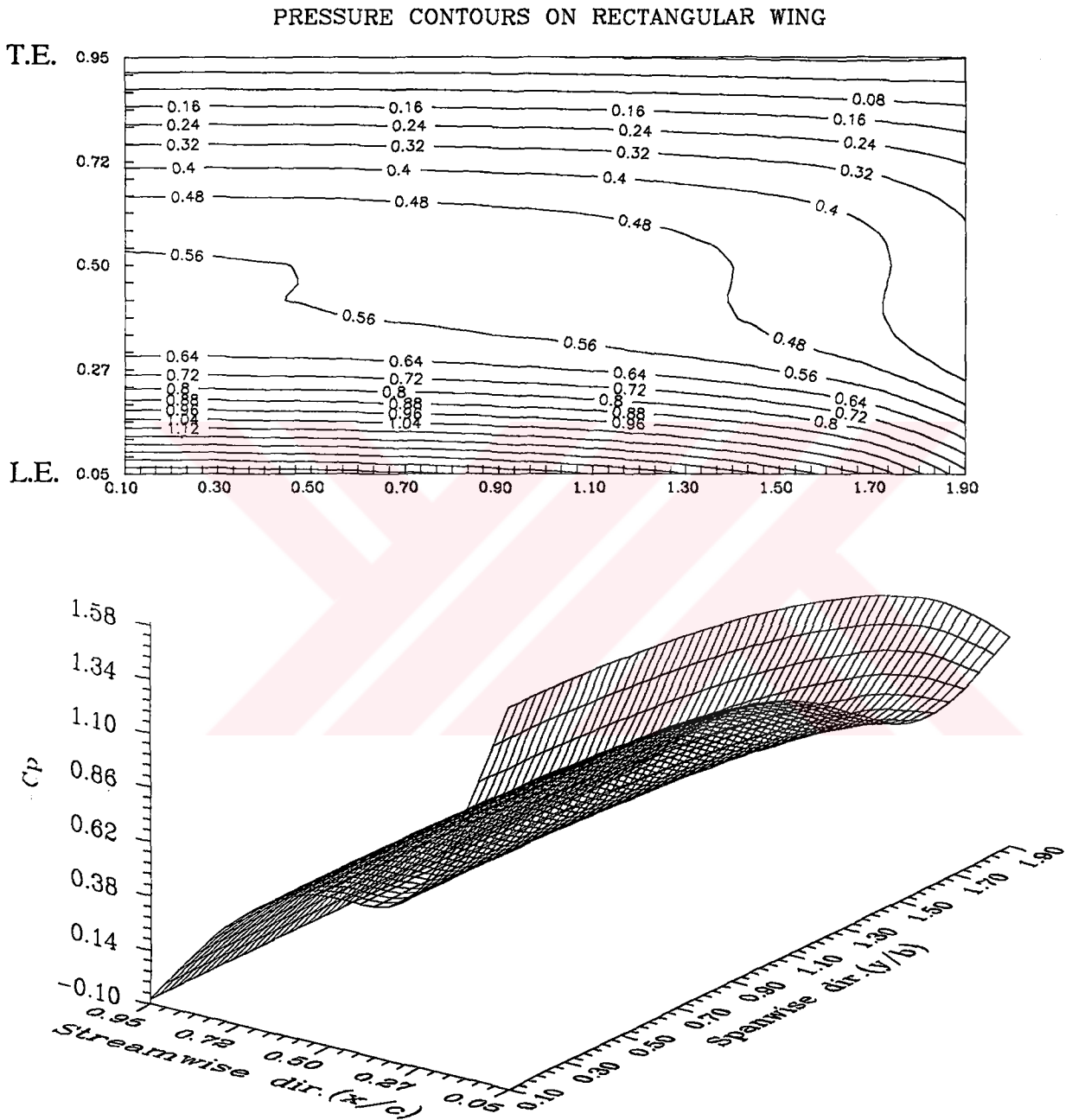
Figure 22.   3-D graphical representation and topology contours of the
pressure coefficient distribution on the upper surface of the wing
at 10° angle of attack at M = 0.4

PRESSURE CONTOURS ON RECTANGULAR WING
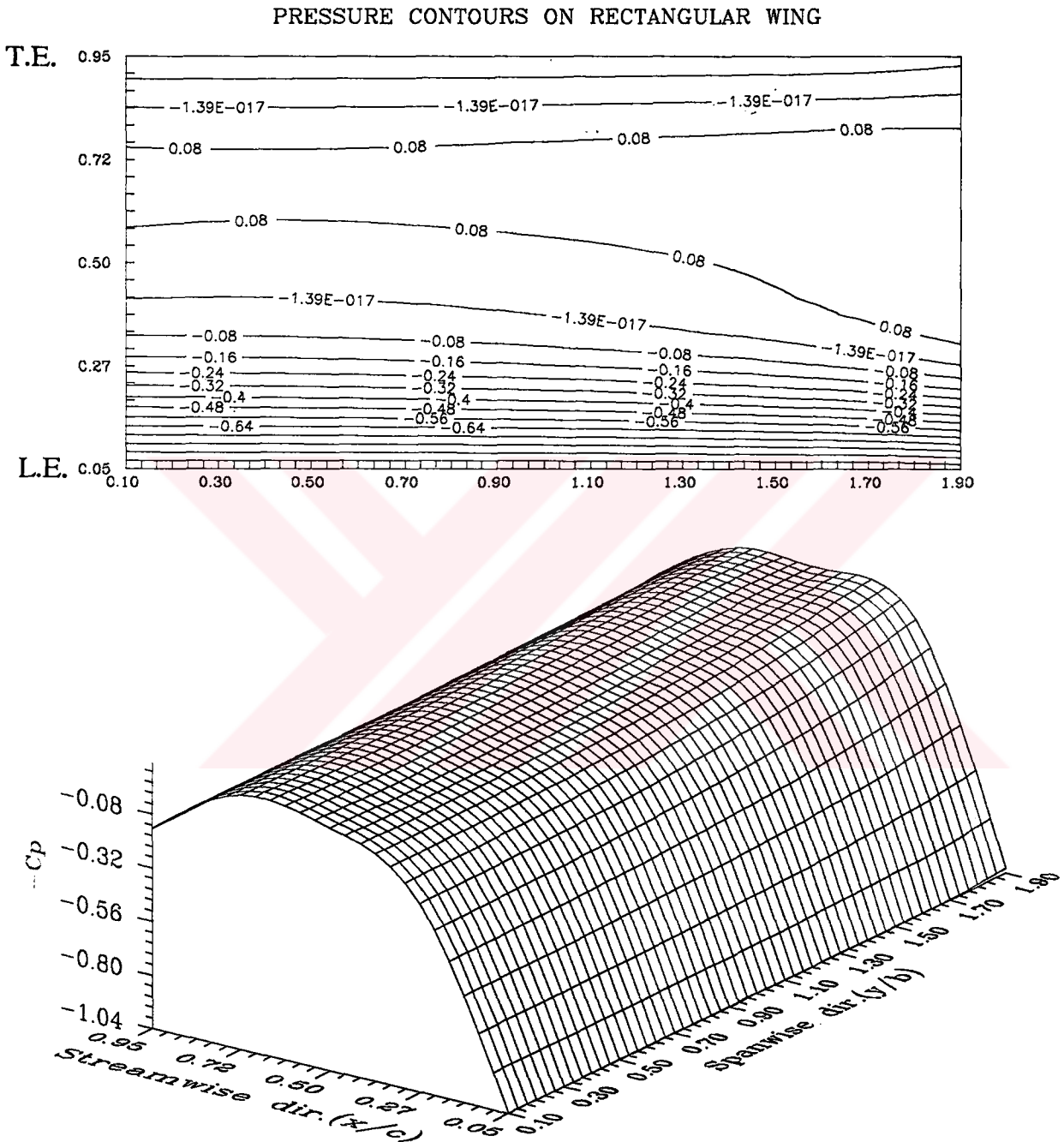
Figure 23.   3-D graphical representation and topology contours of the
            pressure coefficient distribution on the lower surface of the wing
            at 10° angle of attackat M = 0.4

PRESSURE CONTOURS ON RECTANGULAR WING
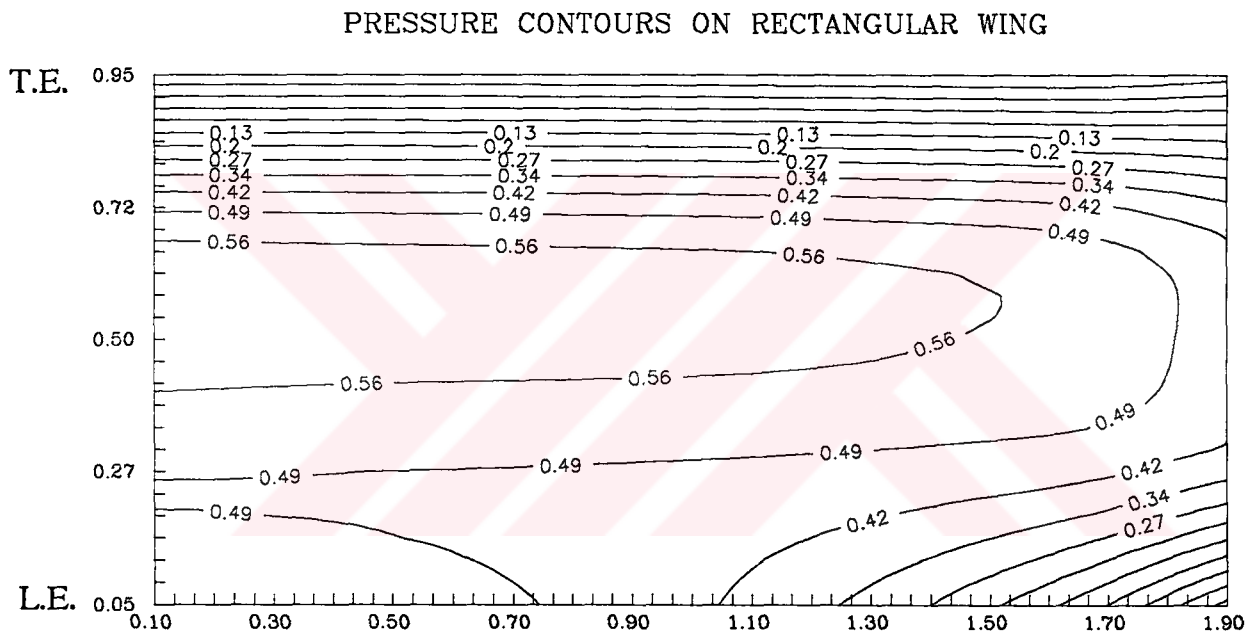
Figure 24.   Pressure differences between upper and lower surface of the
wing at 10° angle of attack at M=0.4
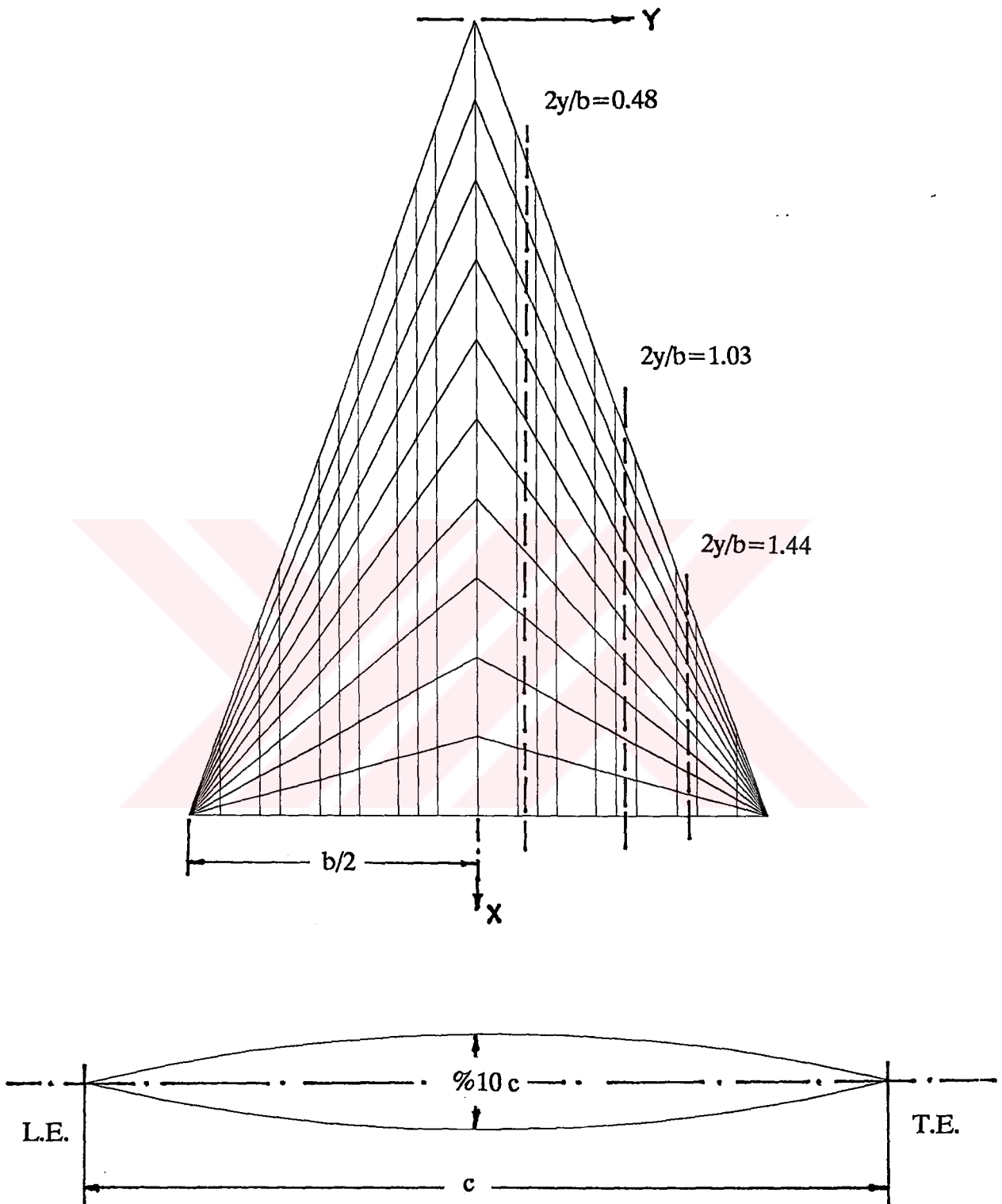
Figure 25.   Geometric definition of delta wing with 70° swept angle.

M=0.4   M=0.6

(a)

(b)

(c)

Figure 26.   Pressure distribution over the delta wing with 0° angle of attack
              at different locations
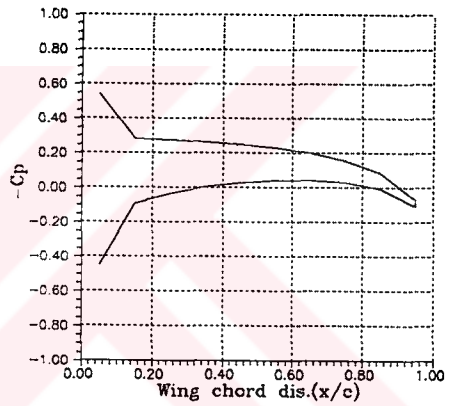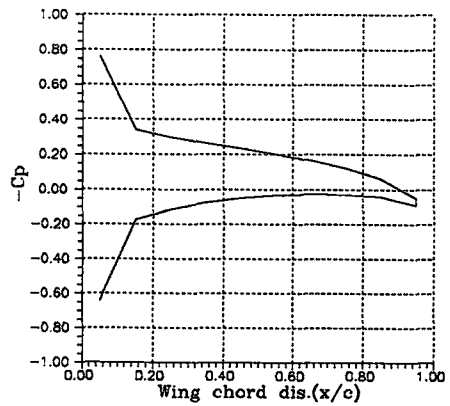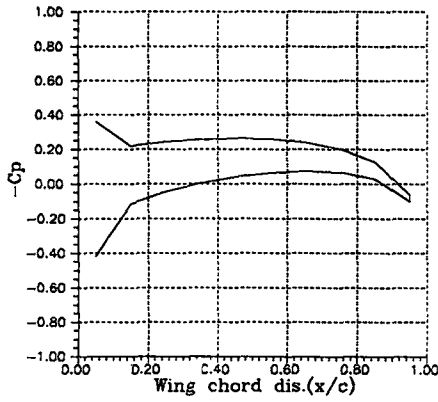   (a) 2y/b = 0.48   (b) 2y/b = 1.03   (c) 2y/b = 1.44
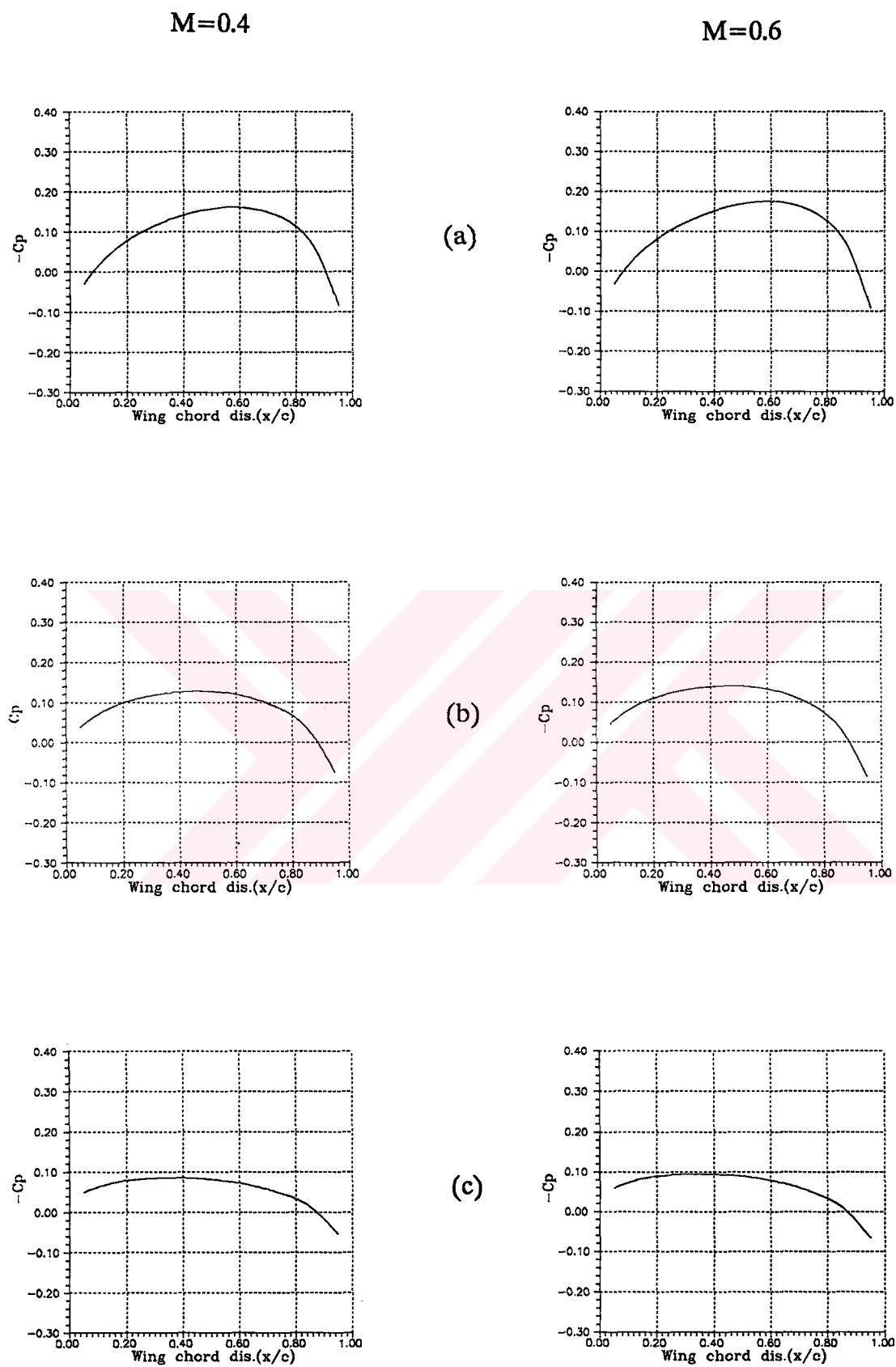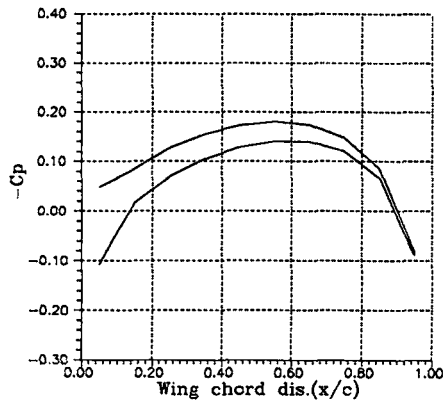
M=0.4   M=0.6

(a)
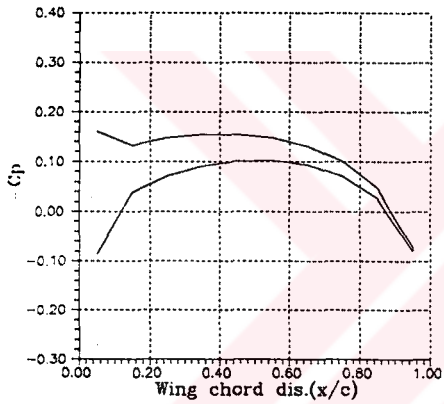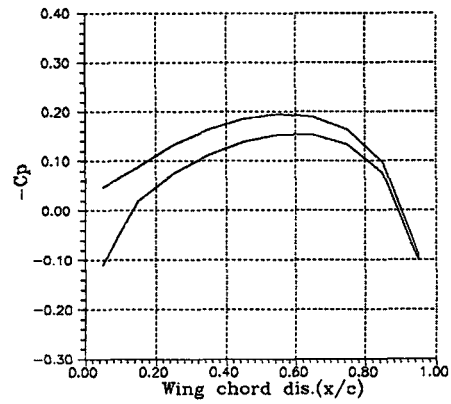
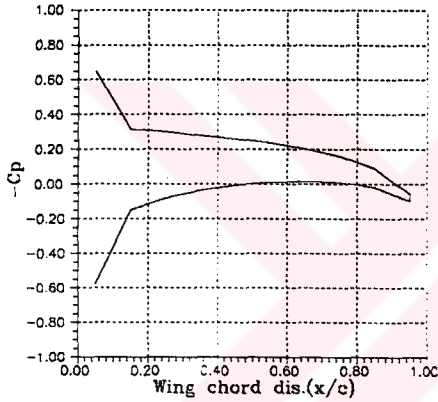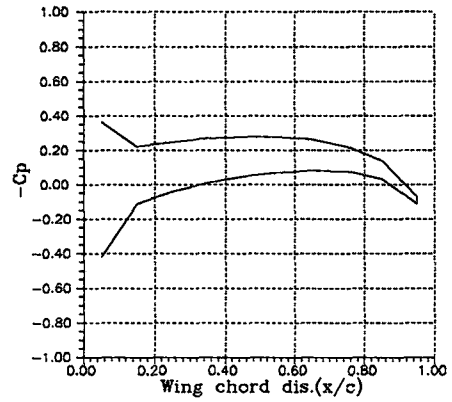(b)
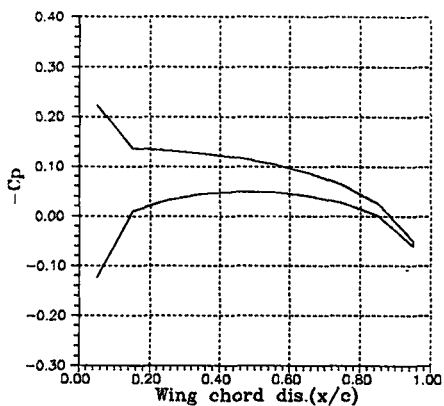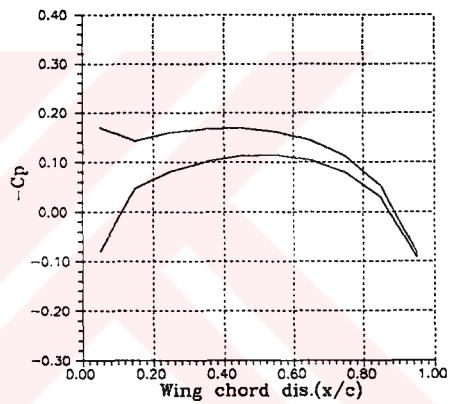
(c)
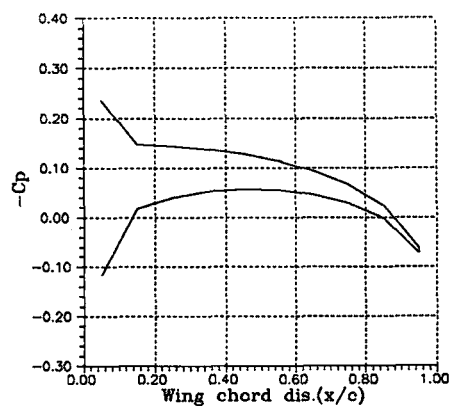
Figure 27.   Pressure distribution over the delta wing with 2° angle of attack
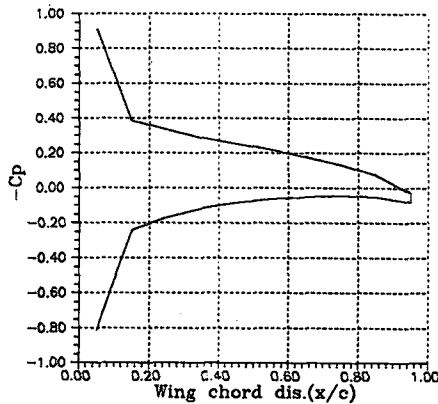   at different locations
            (a) 2y/b = 0.48   (b) 2y/b = 1.03   (c) 2y/b = 1.44

M=0.4   M=0.6

(a)

(b)

(c)

Figure 28.   Pressure distribution over the delta wing with 4° angle of attack
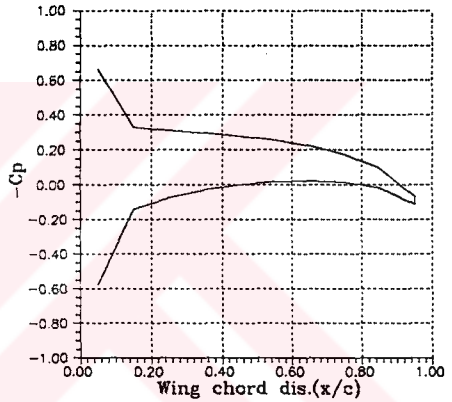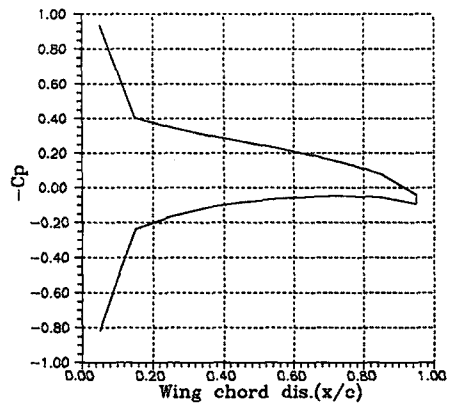   at different locations
            (a) 2y/b = 0.48   (b) 2y/b = 1.03   (c) 2y/b = 1.44

M=0.4   M=0.6

(a)

(b)

(c)

Figure 29.   Pressure distribution over the delta wing with 6° angle of attack
at different locations

(a) 2y/b = 0.48   (b) 2y/b = 1.03   (c) 2y/b = 1.44
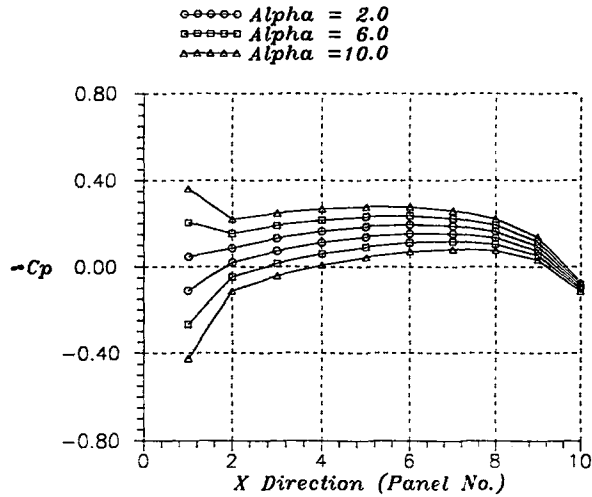
M=0.4　　　　　　　　　　　M=0.6

(a)
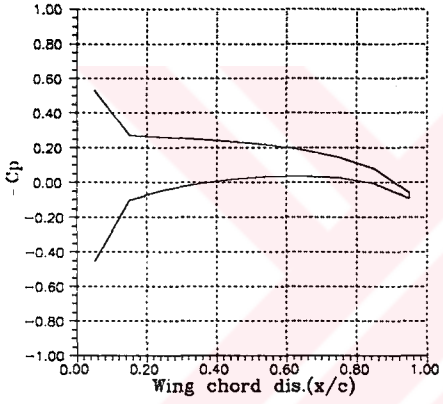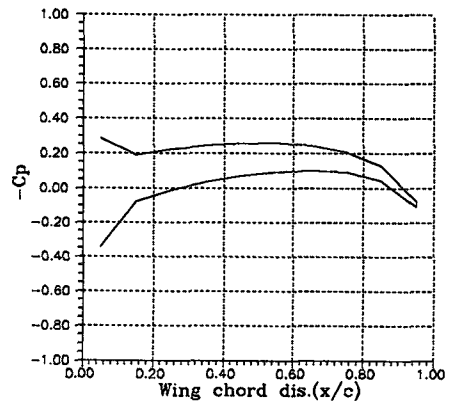
(b)
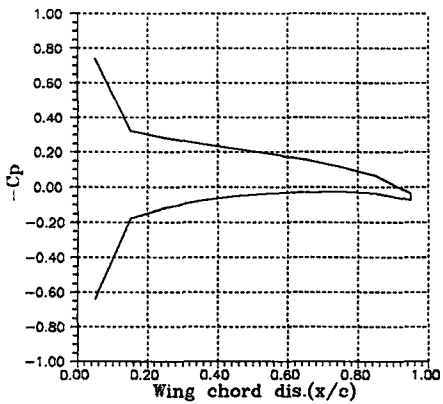
(c)

Figure 30.　Pressure distribution over the delta wing with 8° angle of attack
at different locations
(a) 2y/b = 0.48　　(b) 2y/b = 1.03　　(c) 2y/b = 1.44
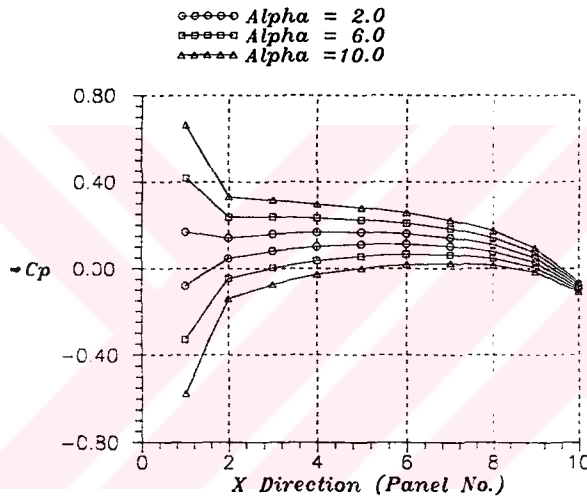
M=0.4

M=0.6

(a)

(b)

(c)

Figure 31.   Pressure distribution over the delta wing with 10° angle of attack
at different locations
(a) 2y/b = 0.48   (b) 2y/b = 1.03   (c) 2y/b = 1.44

PRESSURE DISTRIBUTION AROUND DELTA WING
(Mach = 0.6, y = 0.0873)

o-o-o-o-o Alpha = 2.0
o-o-o-o-o Alpha = 6.0
▲-▲-▲-▲-▲ Alpha =10.0

PRESSURE DISTRIBUTION AROUND DELTA WING
(Mach = 0.6, y = 0.1872)

o-o-o-o-o Alpha = 2.0
o-o-o-o-o Alpha = 6.0
▲-▲-▲-▲-▲ Alpha =10.0

PRESSURE DISTRIBUTION AROUND DELTA WING
(Mach = 0.6, y = 0.2620)

o-o-o-o-o Alpha = 2.0
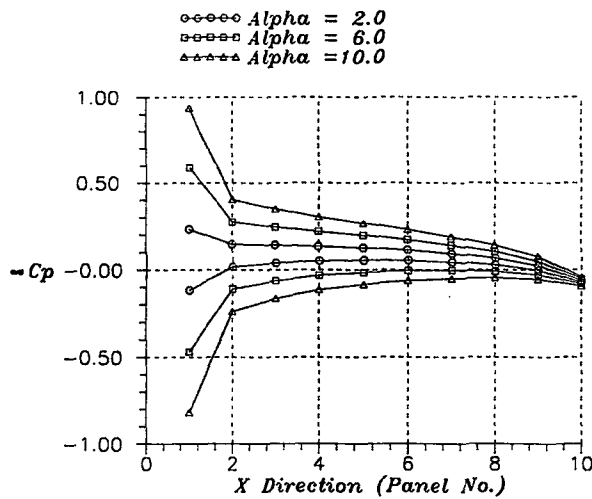o-o-o-o-o Alpha = 6.0
▲-▲-▲-▲-▲ Alpha =10.0

Figure 32.   Pressure distribution evaluation with the angle of attack around
70° swept delta wing at some different locations
(a) 2y/b = 0.48   (b) 2y/b = 1.03   (c) 2y/b = 1.44

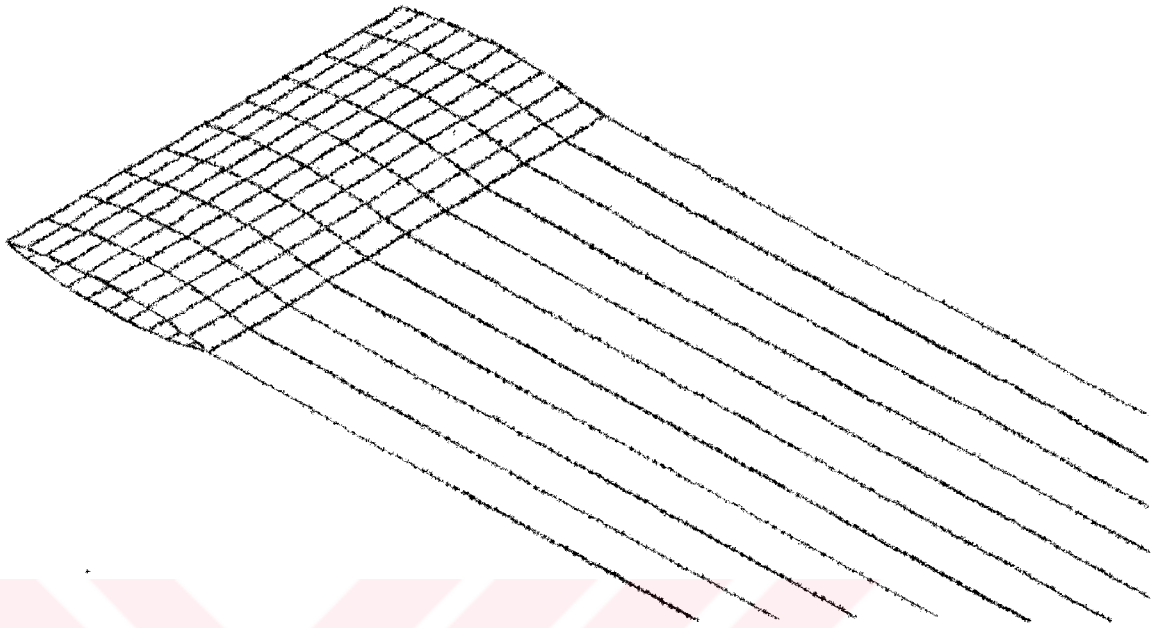Figure 33. Classical wake development at steady state solution with WAERO around the rectangular wing (Mach number is 0.6 and angle of attack is $0°$).
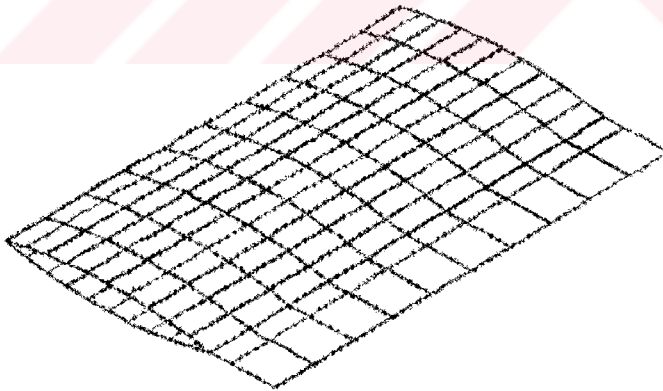

Figure 34. Wake development at unsteady state solution with WAERO around the rectangular wing (Mach number is 0.6 and angle of attack is $0°$).
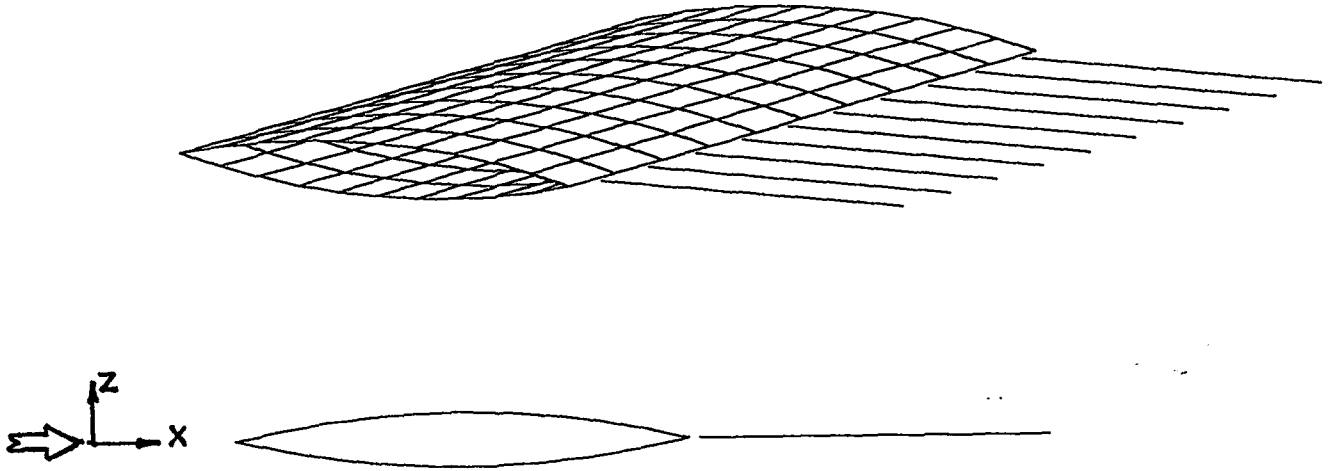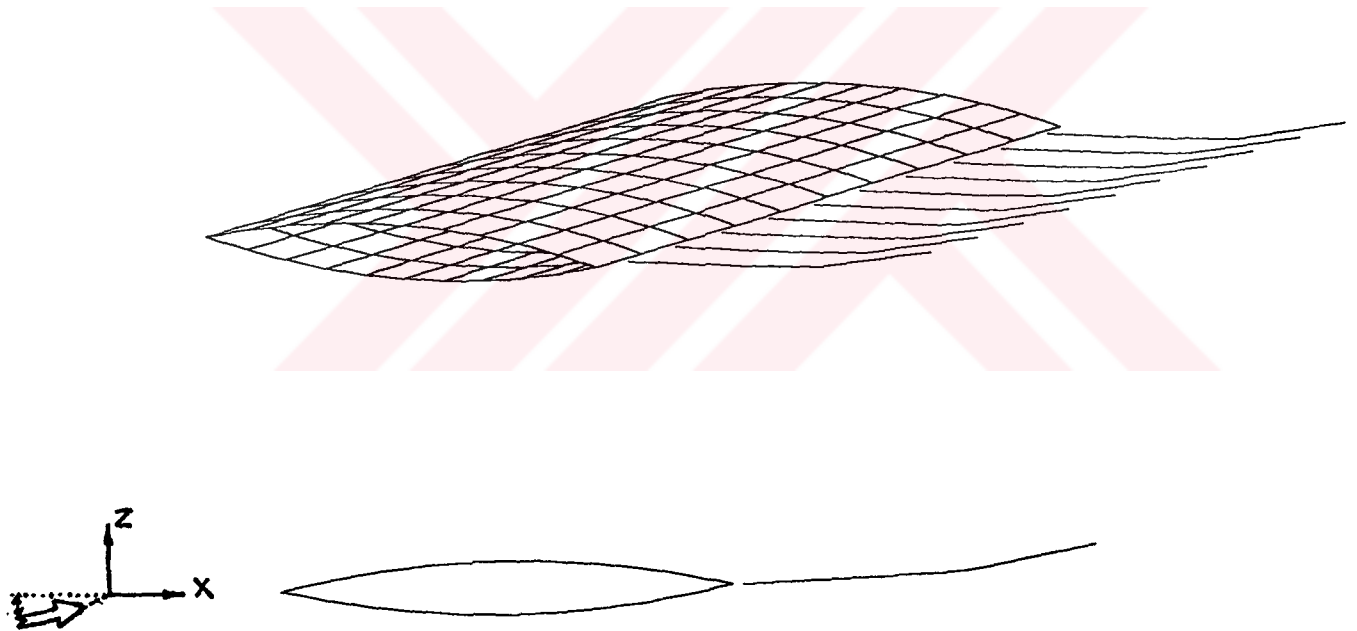
Figure 35-(a). Wake development after three time steps at unsteady state solution around the rectangular wing (Mach number is 0.6, angle of attack is 0 and Dt=0.05)

(b).Wake development after three time steps at unsteady state solution around the rectangular wing (Mach number is 0.6, angle of attack is 4 and Dt=0.05)
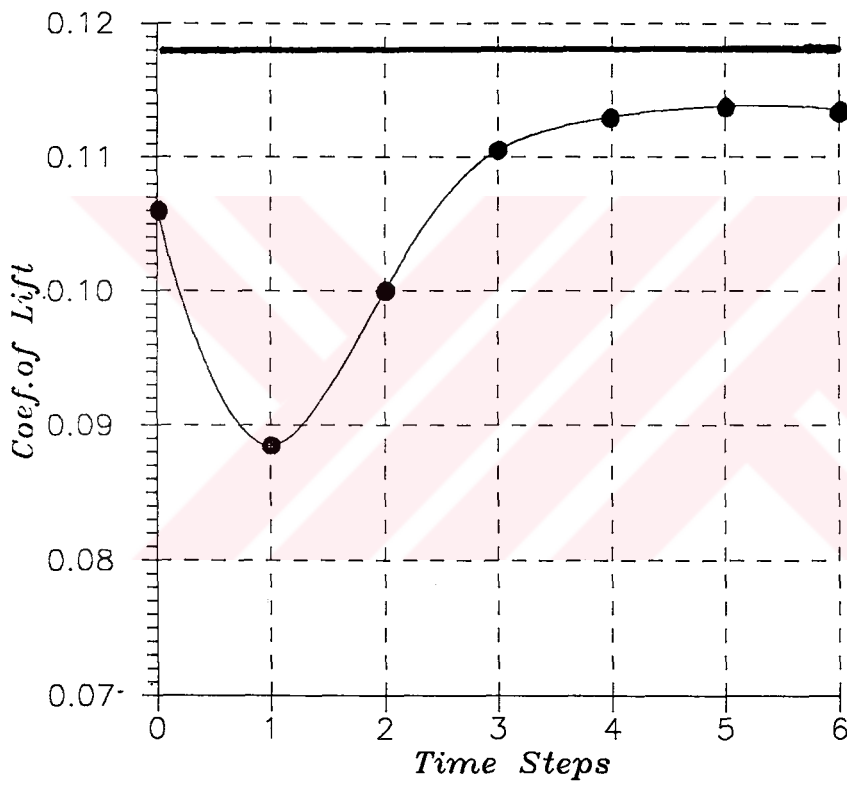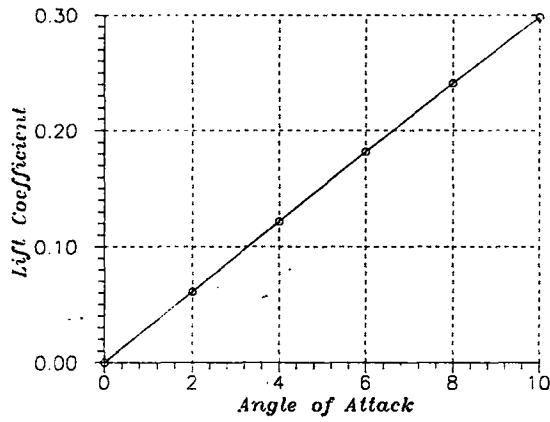
Figure 36. Comparison of Steady State solution between Unsteady State solution according to the Lift Coefficient at the rectangular wing (Mach number is 0.6 and angle of attack is 4, unsteady state solution includes six time steps, the straight line is Steady State Lift Coefficient)

LIFT COEFFICIENT vs. ALPHA DIAGRAM
(Mach = 0.6)

DRAG COEFFICIENT vs. ALPHA DIAGRAM
(Mach = 0.6)
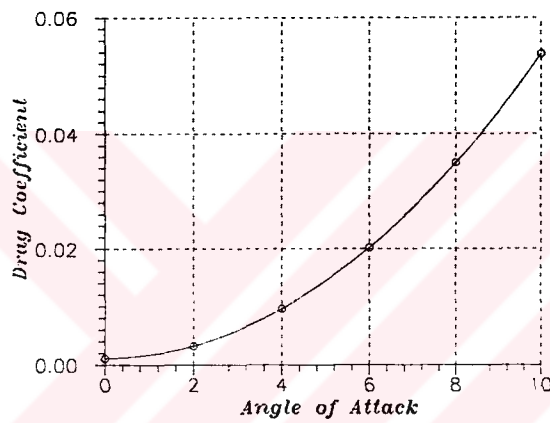
ROLLING MOM.COEF. vs. ALPHA DIAGRAM
(Mach = 0.6)
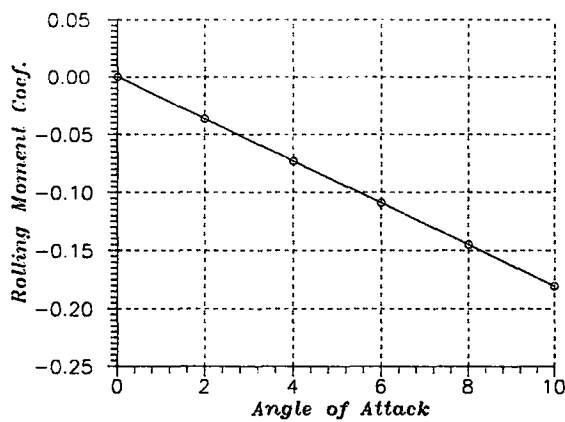

Figure 37. Aerodynamic characteristics behaviour with angle of attack at steady state solutions of WAERO

(a) Lift Coefficient vs. Angle of Attack

(b) Drag Coefficient vs. Angle of Attack
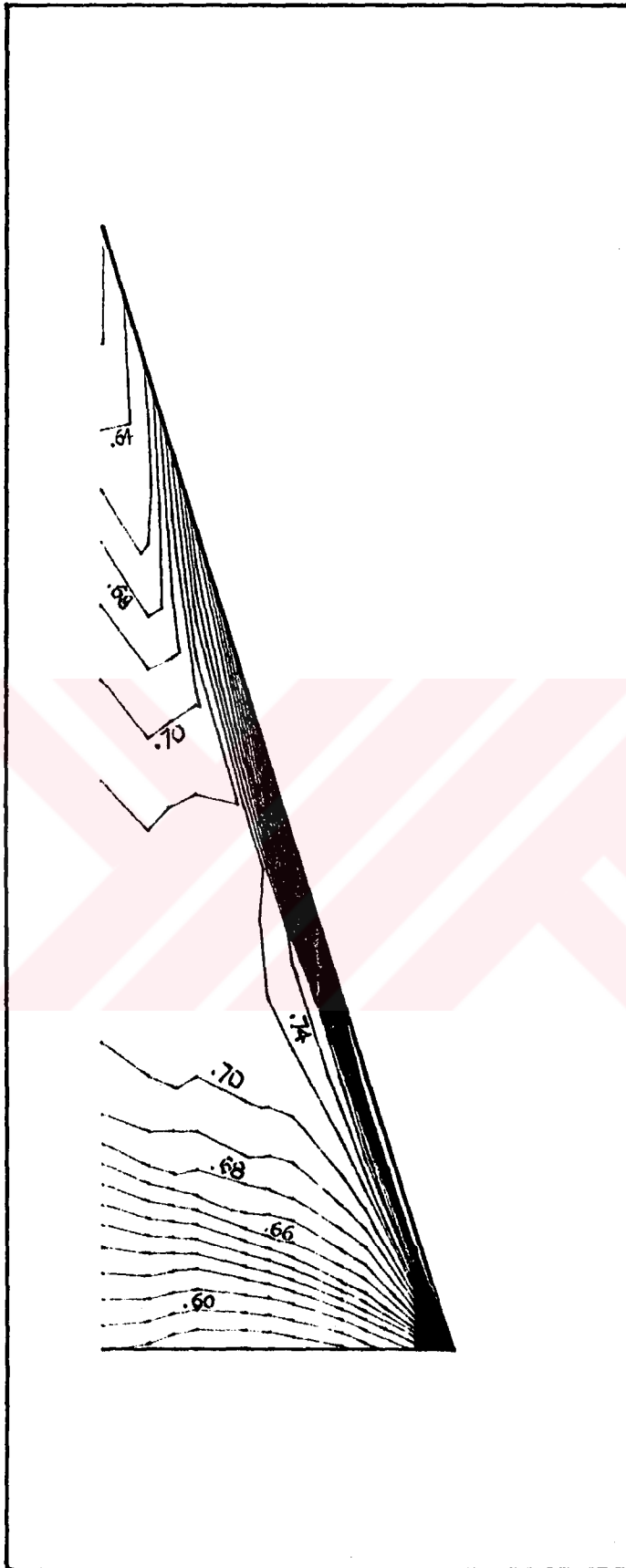
(c) Rolling Moment Coefficient vs. Angle of Attack

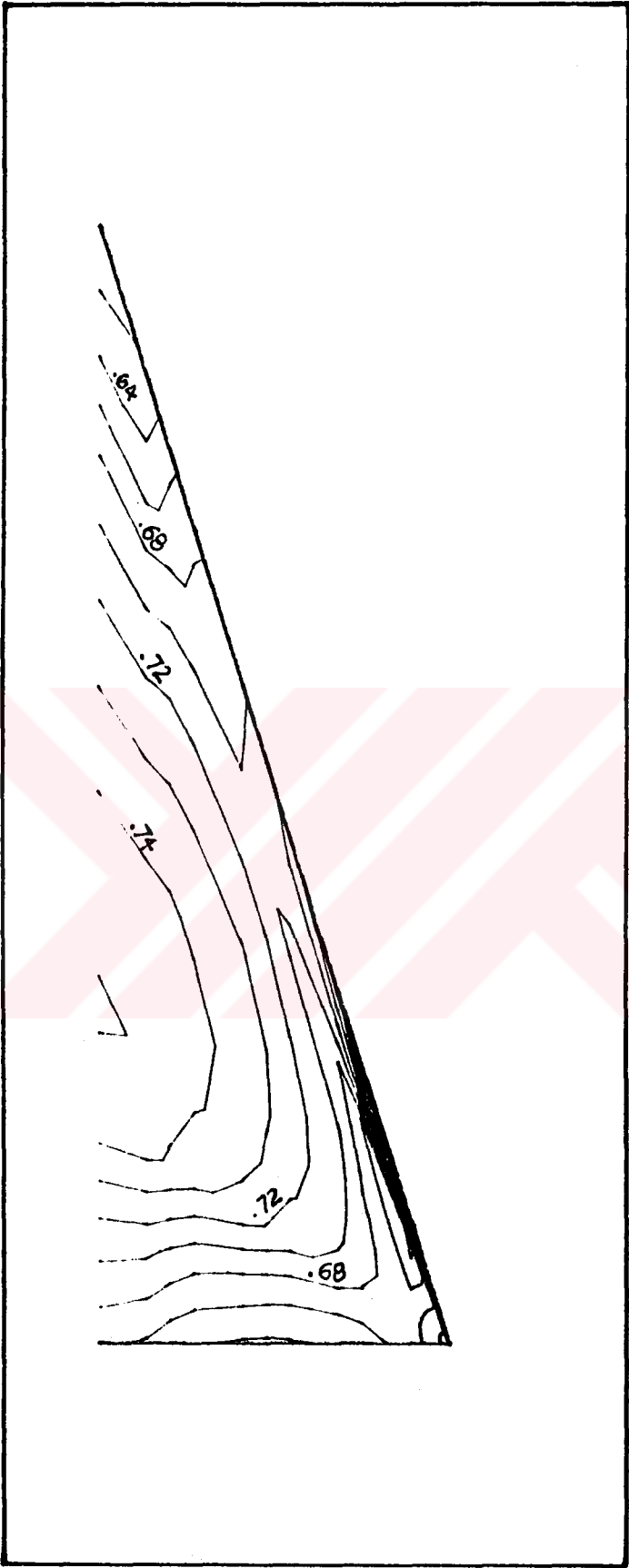Figure 30. Mach contours on the upper surface of the delta wing at M = 0.6

Figure 39. Mach contours on the lower surface of the delta wing at M = 0.6

REFERENCES

[1] **LACAU R.G.**, An Introduction to Tactical Missile Aerodynamics, AGARD R 754, Reference 1, 1987.

[2] **HOEIJMAKERS H.W.M.**, Panel Methods in Aerodynamics: Some Highlights, NLR MP 87028 U, 1987.

[3] **KATZ J., MASKEW B.**, Unsteady Low-Speed Aerodynamics Model for Complete Aircraft Configurations, Journal of Aircraft, Vol.25, No.4, pp. 302-310, 1988.

[4] **CHAPMAN D.R.**, Computational Aerodynamics Development and Outlook, AIAA Journal, Vol.17, No.12, pp. 1293-1313, 1979.

[5] **WOODWARD F.A.**, Analysis and Design of Wing-Body Combinations at Subsonic and Supersonic Speeds, Journal of Aircraft, Vol.5, No.6, pp. 528-534, 1968.

[6] **WILLIAMS B.R., KORDULLA W., BORSI M., HOEIJMAKERS H.M.**, Comparison of Solution of Various Euler Solvers and One Navier-Stokes Solver for the Flow About a Sharp-Edged Cropped Delta Wing, AGARD FDP Vortex Flow Aerodynamics, Scheveningen, Netherlands, 1990.

[7] **KAYNAK Ü., TU E.**, Nonequilibrium Turbulence Modeling Effects on Transonic Vortical Flows About Delta Wings, AGRAD FDP Vortex Flow Aerodynamics, Scheveningen, Netherlands, 1990.

[8] **BARON A., BOFFADOSSI M., De PONTE S.**, Numerical Simulation of Vortex Flows Past Impulsively Started Wings, AGARD FDP Vortex Flow Aerodynamics, Scheveningen, Netherlands, 1990.

[9] **AHMED S.R.**, Fuselage Aerodynamics Design Issues Part II: Theoretical Methods, AGARD FDP Aerodynamics of Rotorcraft, Ankara, Turkey, 1990.

[10] **VUILLET A.**, Rotor and Blade Aerodynamic Design, AGARD FDP
Aerodynamics of Rotorcraft, Ankara, Turkey, 1990.

[11] **KANDIL O.A.**, Steady and Unsteady Incompressible Free-Wake
Analysis, lecture on Morino's "Computational Methods in
Potential Aerodynamics", Springer-Verlag, 1985.

[12] **YATES Jr. E.C.**, Unsteady Transonic Flow - Introduction, Current
Trends, Applications, lecture on Morino's "Computational
Methods in Potential Aerodynamics", Springer-Verlag, 1985.

[13] **MASKEW B. et al.**, Prediction of Aerodynamic Characteristic for Wings
With Extensive Separations, AGARD CP-291, 1980.

[14] **JOHNSON F.T., TINOCO E.N.**, Recent Advances in The Solution of
Three-Dimensional Flows over Wings with Leading Edge
Vortex Separations, AIAA Paper 79-0282, 1979.

[15] **LAMAR J.E., LUCKRING J.M.**, Recent Theoretical Developments and
Experimental Studies Pertinent to Vortex Flow Aerodynamics
with a View Toward Design, AGARD CP-247, 1978.

[16] **DJOJODIHARDJO R.H., WIDNALL S.E.**, A Numerical Method for the
Calculation of Nonlinear, Unsteady Lifting Potential Flow
Problems, AIAA Journal, Vol.7, pp.2001-2009, 1969.

[17] **SUMMA J.M.**, Unsteady Potential Flow About Wings and Rotors
Started Impulsively From Rest, Proceedings of Symposium
on Unsteady Aerodynamics, Arizona, pp.741-767, 1975.

[18] **ATTA E.H. et al.**, Unsteady Aerodynamic Loads on Arbitrary Wings
Including Wing-Tip and Leading Edge Separations, AIAA
Paper 77-156, 1977.

[19] **KANDIL O.A. et al.**, Three Dimensional Steady and Unsteady
Asymmetric Flow Past Wings of Arbitrary Planforms,
AGARD CP-227, 1977.

[20] **LEVIN D., KATZ J.**, Vortex Lattice Method for the Calculation of the
Nonsteady Separated Flow Over Delta Wings, Journal of
Aircraft, Vol.18, No.12, pp. 1032-1037, 1981.

[21] **KATZ J.**, Lateral Aerodynamics of Delta Wings with Leading Edge
     Separation, AIAA Journal, Vol.22, No.3, pp.323-328, 1984.

[22] **KATZ J.**, Method for Calculating Wing Loading During Maneuvering
     Flight along a Three-Dimensional Curved Path, Journal of
     Aircraft, Vol.16, No.11, pp. 739-741, 1979.

[23] **HESS J.L.**, Calculation of Potential Flow About Arbitrary Three-
     Dimensional Lifting Bodies, Douglas Aircraft Co., Report
     MDC J5679 - 01, 1972.

[24] **UCHIDA S., NAKAMURA Y.**, On the Potential Theory of Distributed
     Singularities and Its Edge Condition for a Lifting Flow of Three
     Dimensional Body, Nagoya University, 1974.

[25] **ÖZTÜRK İ.**, A Three Dimensional Method in Linearized Subsonic
     Flow, M.Sc. Thesis, Istanbul Technical University, Institute
     of Science and Technology, Istanbul, Turkey, 1989.

[26] **HOEIJMAKERS H.W.M.**, A Panel Method for the Determination of
     the Aerodynamic Characteristics of Complex Configurations in
     Linearized Subsonic or Supersonic Flow Part II: Evaluation of
     Aerodynamic Influence Coefficients, NLR TR 80124 U, 1980.

[27] **KATZ J., WEIHS D.**, Hydrodynamic Propulsion by Large Amplitude
     Oscillation of an Airfoil with Chordwise Flexibility, Journal of
     Fluid Mechanics, Vol.88, Pt.3, pp.485-498, 1978.

[28] **HOEIJMAKERS H.W.M.**, Panel Methods for Aerodynamic Analysis
     and Design, presented on AGARD FDP Special Course on
     Engineering Methods in Aerodynamic Analysis and Design of
     Aircraft, Ankara, May 1991.

CURRICULUM VITAE

Author was born on May 7, 1968 in Çanakkale, enrolled to Zonguldak Bartın High Scholl in 1982 and graduated with first degree in 1985, the same year enrolled to Istanbul Technical University, Aeronautical and Astronautical Faculty. He finished his undergraduate study with High Honours in 1989 and continued to a graduate study in the Aeronautics and Astronautics department of Institute of Science and Technology of the same university. He is still a research assistant at The Scientific and Technical Research Council of Turkey (TÜBİTAK), Marmara Research Center.